

Stellar Populations in Bulges of Spiral Galaxies^{*}

Bhasker K. Moorthy[†] & Jon A. Holtzman

Department of Astronomy, Box 30001, MSC 4500, New Mexico State University, Las Cruces, NM 88003

Accepted 0000 month 00. Received 0000 month 00; in original form 0000 month 00

ABSTRACT

We present line strengths in the bulges and inner disks of 38 galaxies in the local universe, including several galaxies whose bulges were previously identified as being disk-like in their colors or kinematics, to see if their spectral properties reveal evidence for secular evolution. We find that red bulges of all Hubble types are similar to luminous ellipticals in their central stellar populations. They have large luminosity-weighted ages, metallicities, and α/Fe ratios. Blue bulges can be separated into a metal-poor class that is restricted to late-types with small velocity dispersion and a young, metal-rich class that includes all Hubble types and velocity dispersions. Luminosity-weighted metallicities and α/Fe ratios are sensitive to central velocity dispersion and maximum disk rotational velocity. Red bulges and ellipticals follow the same scaling relations. We see differences in some scaling relations between blue and red bulges and between bulges of barred and unbarred galaxies. Most bulges have decreasing metallicity with increasing radius; galaxies with larger central metallicities have steeper gradients. Where positive age gradients (with the central regions being younger) are present, they are invariably in barred galaxies. The metallicities of bulges are correlated with those of their disks. While this and the differences between barred and unbarred galaxies suggest that secular evolution cannot be ignored, our results are generally consistent with the hypothesis that mergers have been the dominant mechanism responsible for bulge formation.

Key words:

galaxies: bulges – galaxies: stellar content – galaxies: formation – galaxies: evolution – galaxies: spiral – galaxies: ellipticals and lenticular

1 INTRODUCTION

Bulges are important relics of the galaxy formation process. An analysis of their structure, kinematics, dynamics, and stellar content can potentially reveal the physical mechanisms responsible for the formation and evolution of galaxies as well as the nature of the Hubble sequence. Similarities between bulges and ellipticals have long been recognized but recent observations suggest that at least some bulges may be related to disks. This has led to the suggestion that the large bulges of early-type spirals are more similar to ellipticals while late-type bulges are more disk-like (Wyse et al. 1997). As a consequence of these observations, formation scenarios have emerged for bulges that are either identical to those for ellipticals or involve the secular evolution of disks. However, the degree to which formation mechanisms are homogeneous is still open to question.

Early models for elliptical formation involved the monolithic collapse of a primordial gas cloud (Larson 1974; Carlberg 1984; Arimoto & Yoshii 1987). This model naturally explains several observed properties of ellipticals including the mass-metallicity relation and the presence of metallicity gradients but large-scale collapse is inconsistent with present day cold dark matter cosmology and with recent observations showing that massive ellipticals were not fully assembled since after $z=1$ (Bell et al. 2004; Faber et al. 2005). It is now widely believed that ellipticals formed hierarchically through mergers of smaller fragments (Kauffmann et al. 1993). Mergers are frequently caught in the act (van Dokkum et al. 1999; Ferreira & Pastoriza 2004) and photometric and kinematic evidence for past mergers is abundant in ellipticals (Emsellem et al. 2004; van Dokkum 2005). The merger model has been extended to bulges due to the many observed similarities between bulges and ellipticals. For example, Carollo et al. (1997) found that bulges were well-fit by the $R^{1/4}$ law used for ellipticals. The fundamental plane relation of bulges is nearly the same as that of ellipticals, with late-types perhaps lying below early types (Falc3n-Barroso et al. 2002).

^{*} Based on observations obtained with the Apache Point Observatory 3.5-meter telescope, which is owned and operated by the Astrophysical Research Consortium.

[†] E-mail: bmoorthy@nmsu.edu

In the secular evolution scenario, bulges are produced through radial and vertical transport of disk material as the result of instabilities and resonances (see Kormendy & Kennicutt 2004 for a review). These models come in several flavors, most of which involve bars. Simulations that do not include gas have found that bars can buckle, heating the inner disk and increasing its scale height to resemble a bulge. Hydrodynamical simulations have found that bars can transport gas towards the center, triggering intense star-formation (Pfenniger 1993; Friedli & Benz 1995; Norman et al. 1996; Noguchi 2000; Immeli et al. 2004). The presence of neighbors may also drive this (Kannappan et al. 2004). Support for secular evolution comes from observed correlations between the scale lengths of bulges and their disks (Courteau et al. 1996; MacArthur et al. 2003). Recent work has also shown that the light profiles of many bulges are closer to exponential than $R^{1/4}$ (Balcells et al. 2003; MacArthur et al. 2003; de Jong et al. 2004). Furthermore, the ratio of rotational to random motions in bulges is often typical of disks (Kormendy & Illingworth 1982; Kormendy & Kennicutt 2004). Comparisons between the morphology and kinematics of observed galaxies with simulated ones have shown that boxy and peanut-shaped (b/p) bulges are bars viewed at high inclination (Bureau & Freeman 1999; Aronica et al. 2003; Chung & Bureau 2004; Athanassoula 2005). Athanassoula (2005) distinguishes between b/p bulges, which are formed through the buckling of the bar, and what she calls “disky bulges”, which are smaller cold components that formed out of the gas driven inward by the bar.

Bulges that could have been formed through secular evolution are often referred to as “pseudobulges” to distinguish them from the “classical” bulges that may have formed through mergers. Since pseudobulge signatures are generally found in later-typed spirals, Kormendy & Kennicutt (2004) suggest that early-type spirals (Sa’s, Sab’s, and some S0’s) contain classical bulges while late-type spirals (Sb’s, Sc’s and some S0’s) contain pseudobulges. On the theoretical side, Pfenniger (1993) found that secular evolution can produce small bulges but not those having a characteristic radius much larger than the disk scale length. However, it is not at all clear that the spectrum of observed bulge properties points towards two distinct formation scenarios. Since the stability of bars continues to be debated (Shen & Sellwood 2004; Debattista et al. 2004; Bournaud et al. 2005), it is also not clear whether or not pseudobulges should exist only in present-day barred galaxies.

Stellar population (SP) studies can potentially place important constraints on the formation mechanisms. A successful formation scenario has to reproduce the observed distribution of ages and metallicities. In a collapse model, bulges and ellipticals are universally old and have radial metallicity gradients. In his dissipative collapse simulation Carlberg (1984) found that the steepness of the metallicity gradient was correlated with galaxy properties such as mass and luminosity. If ellipticals and bulges formed through mergers, it is important to keep in mind that their assembly histories might be very different from their star formation histories. Λ CDM simulations suggest that most massive ellipticals (and therefore presumably bulges) were not fully assembled until recently ($z < 1$) whereas the bulk of star formation occurred much earlier ($z > 2$) in the progenitor galaxies

(De Lucia et al. 2005). This is consistent with observational studies of merger activity, number counts, and the luminosity function (Faber et al. 2005; van Dokkum 2005). de Lucia et al. find that the star formation histories of massive ellipticals peak at $z \approx 5$ while those of less massive ellipticals peak at progressively smaller redshifts and are more extended. These simulations predict a mass-metallicity relation, with the most massive ellipticals having solar metallicity and the least massive ones being a factor or ten smaller in metallicity. Gradients in SPs are difficult to model within the framework of hierarchical formation. Mergers between disks can presumably preserve existing gradients in the sub-components and produce new gradients through gas infall, but mixing from successive mergers might erase any correlations between gradients and global properties. White (1980) found that the metallicity gradient in a disk galaxy was halved after three mergers with similar sized disks. However, Bekki & Shioya (1999) found that more massive galaxies had steeper metallicity gradients. The impact of secular evolution on gradients is not straightforward. Since the resulting pseudobulge has a smaller scale length than the progenitor disk, an existing disk gradient could become amplified (A Klypin, private communication). However, mixing during secular evolution can have the effect of washing out existing gradients. Adding gas only complicates the picture. If gas is fueled towards the central regions by bars, this could result in a nucleus that is younger and more metal-rich than the outer regions of the bulge. Simulations by Friedli et al. (1994) resulted in a flattening of metallicity gradients in all but the innermost regions where a starburst, fueled by infalling gas, produced a metal-rich nucleus.

Abundance ratios can place additional constraints. Mg and other α -elements are primarily produced in Type II Supernovae (SN II) while a substantial fraction of the Fe-peak elements Fe and Cr are produced in Type Ia Supernovae (SN Ia). Therefore, α -enhancement is generally attributed to a cessation of star formation before the bulk of SN Ia occurred. Through chemical evolution modeling, Thomas et al. (1999) found that a clumpy collapse model produced uniform α -enhancement or positive gradients (increasing α/Fe with radius) while a merger model produced uniformly solar α/Fe or negative gradients. For the case of secular evolution, Immeli et al. (2004) make different predictions for abundance ratios in bulge stars depending on whether it is the gas disk or the stellar disk which first becomes unstable. In the former case, gas clumps merge together and spiral inward, causing massive starbursts and producing large α/Fe ratios. In the latter case, a bar forms and then channels gas towards the center. This occurs on long timescales, resulting in smaller α/Fe ratios.

The only bulges where individual stars can be resolved are those of the Milky Way (MW) and M31. The majority of the stars in the MW bulge are old ($t \geq 7$ Gyr), although young ($t \leq 200$ Myr) and intermediate-age ($200 \text{ Myr} \leq t \leq 7$ Gyr) stars are also detected (Ibata & Gilmore 1995; Sadler et al. 1996; Feltzing & Gilmore 2000; van Loon et al. 2003; Zoccali et al. 2003). As a barred late-type spiral, the MW might be a good candidate for secular evolution but that hypothesis is challenged by the mean stellar age of its bulge. If the bulge were produced through a rearrangement of disk stars, this must have occurred several Gyr ago if the inner disk has the same age distribution as the

disk at the solar neighborhood. The young stars in the bulge are mainly found in the innermost regions. While the gas that formed them could have been driven by a bar, it could just as well have been provided by a recent merger. The mean metallicity of the Galactic bulge is slightly sub-solar (Minniti 1996; Feltzing & Gilmore 2000; van Loon et al. 2003; Zoccali et al. 2003) (Recent Fullbright et al. 2006). The stellar content of M31's bulge is not as well understood as that of the MW since we cannot reach its main sequence turnoff. Observations of giant stars are consistent with M31's bulge being similar in age to the MW bulge and slightly more metal-rich (Rich 1999; Jablonka et al. 2000; Davidge 2001; Stephens et al. 2003; Sarajedini & Jablonka 2005).

SPs in more distant bulges have to be studied through photometry or spectroscopy of integrated light. An important limitation of such studies is that integrated light is dominated by the most luminous stars. Colors have been studied more extensively as they have the advantage of higher signal-to-noise (S/N). Pioneering work by Balcells & Peletier (1994) found that color variations from galaxy to galaxy are much larger than color differences between disk and bulge in each galaxy. Similarly, de Jong (1996) found that bulge and disk colors are correlated and that the color differences between bulge and disk suggested that the SPs did not vary much from one to the other. Unfortunately, color studies suffer from degeneracies between ages, metallicities, and extinction.

Line strengths are nearly insensitive to dust (MacArthur 2005), provide information on the abundances of several elements and molecules, and allow for breaking the age-metallicity degeneracy. Worthey (1994) obtained line strengths for a range of single age, single metallicity SPs (SSPs) on the Lick/IDS system (Burstein et al. 1984; Faber et al. 1985) and found that while individual indices are sensitive to both age and metallicity, the relative sensitivity varies from index to index. Spectral indices have also been defined at high resolution (Vazdekis 1999), allowing better age determinations than otherwise possible. One of the limitations of the original models is that they were calibrated using galactic stars, few of which had abundance ratios different from solar. Much progress has since been made in extending Lick indices to non-solar abundance ratios (Tripicco & Bell 1995; Trager et al. 2000a; Thomas et al. 2003, 2004; Lee & Worthey 2005).

Line strengths have been used extensively to characterize the SPs of ellipticals. The luminosity-weighted ages of cluster ellipticals are large while those of field ellipticals are on average smaller, with a large spread (Rose et al. 1994; Trager et al. 2000a; Vazdekis et al. 2001; Proctor & Sansom 2002; Denicoló et al. 2005; Thomas et al. 2005). This goes against the collapse model and confirms, at least qualitatively, the prediction of the merger model by Kauffmann (1996). Mg-sensitive indices in ellipticals are more tightly correlated with central velocity dispersion than Fe-sensitive indices, resulting in a correlation between Mg/Fe and σ_0 (Bender et al. 1993). Worthey & Colobert (2003) found that the Mg- σ relation of ellipticals is consistent with these objects having been formed through around 50 mergers with merger probability constant or mildly declining with time.

There have been fewer studies of line strengths in

bulges. Integrated light studies on the bulges of the MW and M31 have arrived at similar ages and metallicities as the resolved studies (Puzia et al. 2002, 2005). Both bulges have large SSP ages. M31 is slightly super-solar in SSP metallicity while the Milky Way is solar. Both are α -enhanced with M31 being more so in line with its larger σ_0 . Early studies on extragalactic bulges found them to be similar to ellipticals in their central line strengths (Jablonka et al. 1996; Idiart et al. 1996). Proctor & Sansom (2002) found that bulges have smaller average luminosity-weighted age than ellipticals. These authors did not find the correlation predicted by Kauffmann (1996) for bulges and suggested that it might have been erased by secular evolution in late-types. The largest sample of bulges to date was that of Prugniel et al. (2001), who identified three classes of bulges: a) young bulges which are small, have ionized gas, low velocity dispersions, and low metallicity; b) old bulges that are alpha-enhanced and follow the mass-metallicity relation of ellipticals; and c) bulges that have a mixture of young and old populations, which are less alpha-enhanced than those of class (b), and deviate from the Mg₂ relation of ellipticals. Prugniel et al. and Proctor et al. found that both Fe and Mg were correlated with σ_0 in bulges, resulting in the lack of a tight correlation between Mg/Fe and σ_0 in bulges. Prugniel et al. (2001) found that Mg₂ in bulges is more tightly correlated with the V_{max} of the disk than with σ , indicating that the SPs are more sensitive to the total galaxy potential (i.e. the dark matter halo) than the bulge potential.

Studies with spatial resolution offer several advantages to studies that only sample the central region. First, differential studies of ages and abundances are more reliable than absolute estimates. Second, formation models invariably make predictions for the global properties of galaxies which are better traced by mean observed quantities than central ones; observations with spatial resolution allow estimation of mean values. Finally, as mentioned already, population gradients can place additional constraints on formation mechanisms.

Line strength gradients have been studied extensively in ellipticals. Carollo et al. (1993) and Forbes et al. (2005) find strong correlations between gradients and physical properties while others find weak (Mehlert et al. 2003) or no (Kobayashi & Arimoto 1999) correlations. There have been relatively few studies on gradients in bulges. Fisher et al. (1996) found steeper metallicity gradients along the minor axes of nine edge-on S0s than along the major axes, suggesting different formation mechanisms for the bulge and the disk. Goudfrooij et al. (1999) found that gradients were correlated with luminosity in 16 bulges. Proctor et al. (2000) found that gradients correlated with velocity dispersion, albeit with a sample of only four galaxies, while Jablonka et al. (2002) found no such correlation. Integral field spectroscopy has enabled the acquisition of 2D line strengths in bulges with results just starting to emerge (e.g. Sil'chenko et al. 2003; Falcón-Barroso et al. 2004). Recent work by Ryder et al. (2005) shows that tunable filters might be another way to obtain 2D line strengths.

In this paper, we present line strengths and line strength gradients in the bulges and inner disks of 38 galaxies. Our sample, described in Section 2, was chosen to span a range of bulge properties and specifically targeted several galaxies

with blue bulges and similar bulge/disk colors and/or disk-like kinematics in an attempt to look for SP signatures of secular evolution. Section 3 describes the observations and data analysis. Section 4 describes the SP results and Section 5 discusses their implications for bulge formation scenarios. Section 6 contains a summary. The structure, kinematics, and dynamics and how they relate to the SPs will be discussed in a future paper (hereafter Paper II).

2 THE GALAXY SAMPLE

We selected a sample that included some bulges that are similar in color to their disks and others that are considerably redder as a control. Color was chosen as the primary selection criterion because this has so far been the best studied property of bulges. de Jong (1996, hereafter DJ) and Peletier & Balcells (1997, hereafter PB) obtained color gradients of galaxies from the Uppsala General Catalog (Nilson 1973) with major axes larger than $2'$. We selected 17 galaxies PB and 14 from DJ. The two samples complement each other nicely in their sky coverage and sampling of Hubble types. The DJ galaxies are nearly face-on while the PB galaxies are highly inclined.

We also included three galaxies, NGCs 2787, 3384, and 3945, which were previously found to possess disk-like structural and kinematic properties (Busarello et al. 1996; Sil'chenko et al. 2003; Pinkney et al. 2003; Erwin et al. 2003). All three are barred S0 galaxies with inner disks or bars that are more luminous than the surrounding bulge. One of the PB galaxies, NGC 7457, is also known to have disk-like kinematics (Kormendy 1993; Pinkney et al. 2003). Michard & Marchal (1994) found small bar-like distortions in this galaxy and Emsellem et al. (2004) found nearly cylindrical rotation which is seen in boxy bulges (Bertola & Capaccioli 1977; Kormendy & Illingworth 1982; Falc3n-Barroso et al. 2004) and in simulations of edge-on bars (Combes et al. 1990; Sellwood 1993; Athanassoula & Misiriotis 2002).

This project initially began in collaboration with some members of the ENEAR survey (Wegner et al. 2000). Therefore, the first five galaxies we observed were from their sample: NGCs 4472, 2775, 3544, 3831, and 5793. NGC 4472, a bright elliptical in the center of the Virgo cluster, was included for comparison with previous studies. The other four galaxies were selected to span a wide range in inclination and bulge-to-disk ratio.

There are several reasons for including both high- and low-inclination galaxies:

1. Minor axis observations of highly inclined galaxies offer minimum disk contamination in the outer regions of the bulge.
2. In moderately inclined galaxies, there is actually more disk contamination along the minor axis than the major axis for the same solid angle. To estimate the degree of disk contamination, we obtained spectra along both major and minor axes for some of our inclined galaxies.
3. Major axis observations of inclined galaxies allow for the measurement of rotation which can provide additional information about the structure of the galaxy.
4. Low-inclination galaxies have less disk contamination in the central regions and allow for clear identification of

bars, rings, and other morphological features. Including both high- and low-inclination galaxies allows for a comparison between bars and b/p bulges.

5. In highly-inclined galaxies, the bulge and disk can be distinguished based on their shapes (spheroidal versus flat). In face-on galaxies, this is not possible and so bulges are generally defined as the excess light on top of the inward extrapolation of an exponential disk. SPs and kinematics offer two additional and independent means of distinguishing between bulges and disks in face-on galaxies.

Twelve out of our 20 low-inclination galaxies are barred. Some of our highly-inclined galaxies were classified by Lütticke et al. (2000) into peanut-shaped, boxy, nearly boxy, or elliptical bulges. For our remaining highly-inclined galaxies, we determined the shapes using their technique. This yielded 10 b/p bulges and 8 elliptical bulges. Therefore the fraction of barred galaxies in low-inclination galaxies is approximately equal to the fraction of b/p bulges in highly-inclined galaxies. While peanut-shaped bulges are easily identified, it is not always easy to distinguish an elliptical bulge from one that is slightly boxy. For instance, Lütticke et al. classify NGC 5838's bulge as elliptical but Michard & Marchal (1994) describe it as boxy.

Table 1 contains basic data on our galaxies. The column "Morph." describes the shape of the bulge if the galaxy is highly-inclined (Boxy, Peanut, or Elliptical) and whether or not it is barred if it is not highly-inclined. Identifications marked with an asterisk are those of Lütticke et al. while those without asterisks are our identifications.

When comparing SPs in galaxies with different colors, it is important to keep in mind that color is correlated with the global dynamical properties of a galaxy. Fig. 1 shows the bulge B-K colors as a function of central velocity dispersions, and maximum disk rotational velocities of our galaxies where available. We found that it is useful to subdivide bulges according to whether they are redder or bluer than B-K=4; these are shown as red and blue points. In this and subsequent plots, point shape represents the Hubble type: circles are S0's; hexagons are S0a's and Sa's; pentagons are Sab's; squares are Sb's; and triangles are Sbc's and Sc's. Filled symbols are barred galaxies. Thin open symbols are elliptical bulges if highly-inclined and unbarred galaxies if not highly-inclined. Thick open symbols are b/p bulges.

Bulge colors correlate more tightly with V_{max} than with σ_0 . Galaxies with $V_{max} > 200 \text{ km s}^{-1}$ host red bulges while those with $V_{max} < 165 \text{ km s}^{-1}$ host blue bulges. Both red and blue bulges are found in nearly the full range of central velocity dispersions spanned by our galaxies although there is an overabundance of red bulges in large σ galaxies and vice versa.

3 OBSERVATIONS AND DATA ANALYSIS

3.1 Observations

Observations were made with the Double Imaging Spectrograph (DIS) on the ARC 3.5m telescope at Apache Point Observatory between January 2000 and February 2004. The spectrograph uses a dichroic to split the light into separate blue and red channels. During this period, the instrument was upgraded in several phases with the installation of new

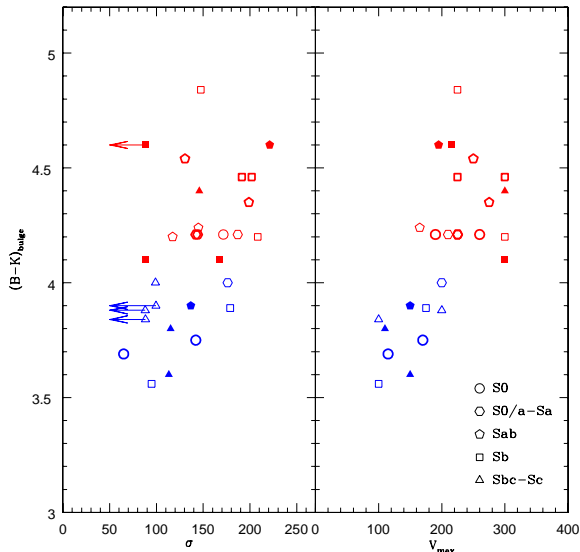


Figure 1. Bulge color versus central velocity dispersion and maximum disk rotational velocity. The velocities are from this work while the colors are from PB and DJ. The central velocity dispersions were measured within an aperture of approximately 4 arcsec. See Table 1 for the definition of bulge color. Bulges are shown in red or blue according to whether they are redder or bluer than $B-K=4$. Filled symbols are barred galaxies. Thin open symbols are elliptical bulges if highly-inclined and unbarred galaxies if not highly-inclined. Thick open symbols are b/p bulges.

detectors and optics. Table 2 gives the specifications of each configuration and Table 3 describes the spectroscopic observations. DIS I gave us continuous wavelength coverage from 4000 to 7500 Å while DIS II and DIS III gave us continuous coverage from 3700 to 7500 Å. A 5 arcmin \times 1.5 arcsec slit was used in all the observations. On each night, we observed a quartz lamp for flatfielding, arc lamps for wavelength calibration, and two to five spectrophotometric standards for flux calibration. On several nights, Lick standard stars from Worthey et al. (1994) were observed to allow us to transform our line indices to the Lick/IDS system.

For most of the highly inclined galaxies, we obtained spectra along both major and minor axes. For the unbarred low-inclination galaxies, we obtained major axis profiles except for NGC 2916 for which we obtained a minor axis profile instead because there was a bright star along the major axis. For the clearly barred galaxies, we placed the slit along the bar. For IC 302 and NGC 2487, this is different from the position angle of the major axis. In NGC 5375, the bar happens to be along the major axis. We could not identify a major axis in NGC 266 or NGC 5020 but the slit must have been placed close to it as we see substantial rotation. We did not detect any rotation in five galaxies: IC 302 and NGCs 765, 2487, 2916, and 6246A, due to their inclinations being too low.

We obtained images in B, V, and R for bulge-to-disk decomposition on six nights using the SPIcam detector on the same telescope. Typical exposure times were 600 sec for B, 180 sec for V, and 120 sec for R. Superbiases and twilight flats were obtained on each night.

3.2 Basic Reductions

Data reduction was carried out using the XVISTA software package. For the imaging, basic reduction included bias subtraction and flatfielding. For the spectroscopy, flat-fields were constructed using a median of 5 to 10 bright quartz lamp exposures; the mean spectral response was divided out. Wavelength calibration was performed using He, Ne, and Ar arc lamp exposures, using a fifth order polynomial for both blue and red channels. Flux calibration was performed using a spline fit to published spectra of the spectrophotometric standards (Massey et al. 1988). Line curvature along the slit was measured using the lamp exposures and a simple row by row shift was stored for subsequent correction. Similarly, spatial distortion in the spectrograph was measured using standard star exposures and the correction was stored. Since spatial distortion includes a component due to differential refraction unless the slit is perpendicular to the parallactic angle, this component was calculated and removed from the standard star measurements. Application of a correction to the galaxies includes a refraction component and the spectrograph component.

Each galaxy frame was subtracted by the overscan and superbias, flat-fielded, and trimmed to remove the overscan region. The line curvature and spatial distortion corrections were applied. Multiple observations of each galaxy were then coadded, rejecting cosmic ray outliers in the process. Where multiple observations were not available, cosmic rays were removed by eye using a spatial median filter. Variance frames were propagated throughout the reduction process. To combine the red and blue channels, the red galaxy spectra were rescaled to spatially match the blue spectra. The spectra were then extracted in approximately 1 arcsec bins near the center of the galaxy and using larger bins further out. An average of sky values measured on both sides of the galaxy was subtracted from each slice. Wavelength and flux calibrations were applied and both red and blue frames were rebinned to 3 Å/pixel. Finally, the spectra were deredshifted and the red and blue sides were combined. The blue spectrum was used out to a wavelength of 5600 Å and the red from 5450 Å. In the overlap region between 5450 and 5600 Å, an average of red and blue values was used. In some galaxies, there is a discontinuity in the overlap region that arises from the difficulty of accurately combining the two channels for extended objects; fortunately none of our absorption features fall within this region.

On our last observing run (Feb 15, 2004), the light on star frames was too extended to be explained by seeing alone. The excess light, which we believe is scattered light, had a spectral energy distribution similar to that of the mashed stellar spectrum but without any narrow spectral features presumably because it is significantly defocused. Since adding a constant to a spectrum decreases the equivalent width (EW) of an absorption features and since the relative contribution of the scattered light to galaxy light increases with distance from the galaxy center, this introduces an artificial negative gradient in the line strength profiles. To correct for the scattered light, we fit the 2d stellar spectrum with a smoothed stellar spectrum along the wavelength direction and a fifth order polynomial along the spatial direction, masking out the central 20 pixels (8.4 arcsec). This spatial profile, combined with the smoothed spectral profile

of the galaxy, was subtracted from each galaxy frame. One galaxy that was observed on the problematic night, NGC 3384, has previously measured index profiles. Applying the correction resulted in much better agreement with the published values (see Section 3.7). No scattered light correction was applied on any of the other nights since the correction derived for those nights did not affect the line strength profiles significantly.

3.3 Measuring and Correcting for Rotation and Velocity Dispersion

We measured rotation and velocity dispersion in the stellar components of our galaxies using the pPXF package (Cappellari & Emsellem 2004). SSP spectra were constructed using the SP models by Bruzual & Charlot (2003, hereafter BC03) assuming a Chabrier initial mass function. The pPXF routine fit each galactic extraction with a linear combination of SSP spectra, shifting and broadening these to match the galaxy’s rotation and velocity dispersion respectively. The fit was performed within the wavelength range 4800-5400 Å, with the emission lines H β , [OIII] 4959, and [OIII] 5007 masked out. The profiles will be presented in Paper II.

The galaxy spectrum at each location was shifted by the measured stellar rotation before measuring the line indices. To correct the indices for velocity dispersion, line strengths were measured on an SSP template that was broadened by the measured velocity dispersion and an unbroadened but otherwise identical template. These templates were also constructed using a linear combination of BC03 SSP spectra with emission lines masked out, but the wavelength range for the fit was 4000-6600 Å, to include all the Lick indices. This template was also used for emission correction (following section). The measured absorption line equivalent widths were multiplied by the ratio of the unbroadened line strength to the broadened one; for magnitudes the correction factor is the difference between these two quantities.

3.4 Measuring and Correcting for Emission

Some absorption indices can be severely affected by line-filling by emission. These include the Balmer indices, Fe5015 (due to [OIII] 5007 emission), and Mg_b (due to [NI] 5199 emission). To correct for this, we subtracted the template described in the previous section from each galaxy spectrum. If on the residual spectrum, H α was found to be in emission at the 5 σ level and a local maximum was detected at H β , a gaussian was fit to the H β emission and subtracted from the galaxy spectrum. This procedure was repeated for H γ and H δ . [OIII] 5007 and [NI] 5199 were subtracted out if they were found to be in emission at the 3 σ and 4 σ levels respectively. A larger threshold was used for [NI] 5199 because this feature lies at the edge of the Mg₂ absorption feature and spurious discontinuities often show up there due to template mismatch.

EWs were measured for several emission-lines to study the nature of the ionized gas in bulges and inner disks. The galaxy continuum, obtained by smoothing the galaxy spectrum, was added to the emission spectrum described above before measuring the EWs.

3.5 Lick Index Measurements

The final galaxy spectra were broadened to 9.5 Å FWHM, which is approximately equal to the Lick resolution, and rebinned to a dispersion 0.125 Å/pixel. Variable broadening as prescribed in Worthey & Ottaviani (1997) was tried and found not to produce significantly different results. The strengths of 25 absorption features were measured using the latest bandpasses from Guy Worthey’s webpage. The EW or magnitude of each feature was computed following Trager et al. (1998).

Spectral indices were measured on Lick standard stars, exactly as done for the galaxies, to transform our line strengths to the Lick/IDS system. Such transformations are necessary because our detector differs in resolution from the IDS and because the IDS spectra were not flux calibrated. 24 stars ranging in spectral type from F5V to K7III were used in deriving the transformations for DIS I and 22 stars (also F5V to K7III) were used for DIS III. DIS III transformations were used for DIS II since the same gratings were used for both. From imaging one of the stars at several positions along the slit, it was determined that the line strengths do not vary significantly with slit position. Fig. 2 shows the transformations. The rms scatter when applying the transformations on the stars are shown at the bottom-right of each plot. The flux response of the detector changes rapidly at the long wavelength end of the blue channel, making measurements there difficult. Only the Mg₁ and Mg₂ indices were affected by this, but severely so, since their continuum bandpasses are far apart and the red continuum bandpass lies right where our flux response is steepest. This resulted in large scatter in the transformations of these indices. For the other indices, the scatter in the transformations is similar or slightly larger than that obtained by Proctor & Sansom (2002).

3.6 Comparison with the literature

Fig. 3 shows comparisons of Lick indices between this work and the most recently published values for NGC 4472. There is excellent agreement in the Ca4227, H β , Fe5015, \langle Fe \rangle , and Fe5270 profiles between this work and all the published values. Our other index profiles are systematically offset from at least one of the other two studies but the offset is within the uncertainties of transforming our data to the Lick system. In general, our results agree better with the long-slit data from Vazdekis et al. (1997) than the IFU data from Peletier et al. (1999). Nearly all our central values agree with those of Trager et al. Emission correction was not responsible for any disagreement among studies since NGC 4472 does not have much emission.

The first column of Fig. 4 shows index comparisons between this work (triangles), azimuthally averaged IFU data from Silchenko (1999; asterisks), and SAURON data extracted along the major-axis from Falcón-Barroso et al. (2004; squares) for NGC 7332. All the central values are in agreement. The slope of our H β and Fe5270 profiles are steeper than Falcón-Barroso et al.’s but not as steep as Silchenko’s. Our Mg_b and Fe5015 profiles agree reasonably well with Falcón-Barroso’s but Silchenko’s Mg_b profile is again steeper.

The second column of Fig. 4 shows index comparisons

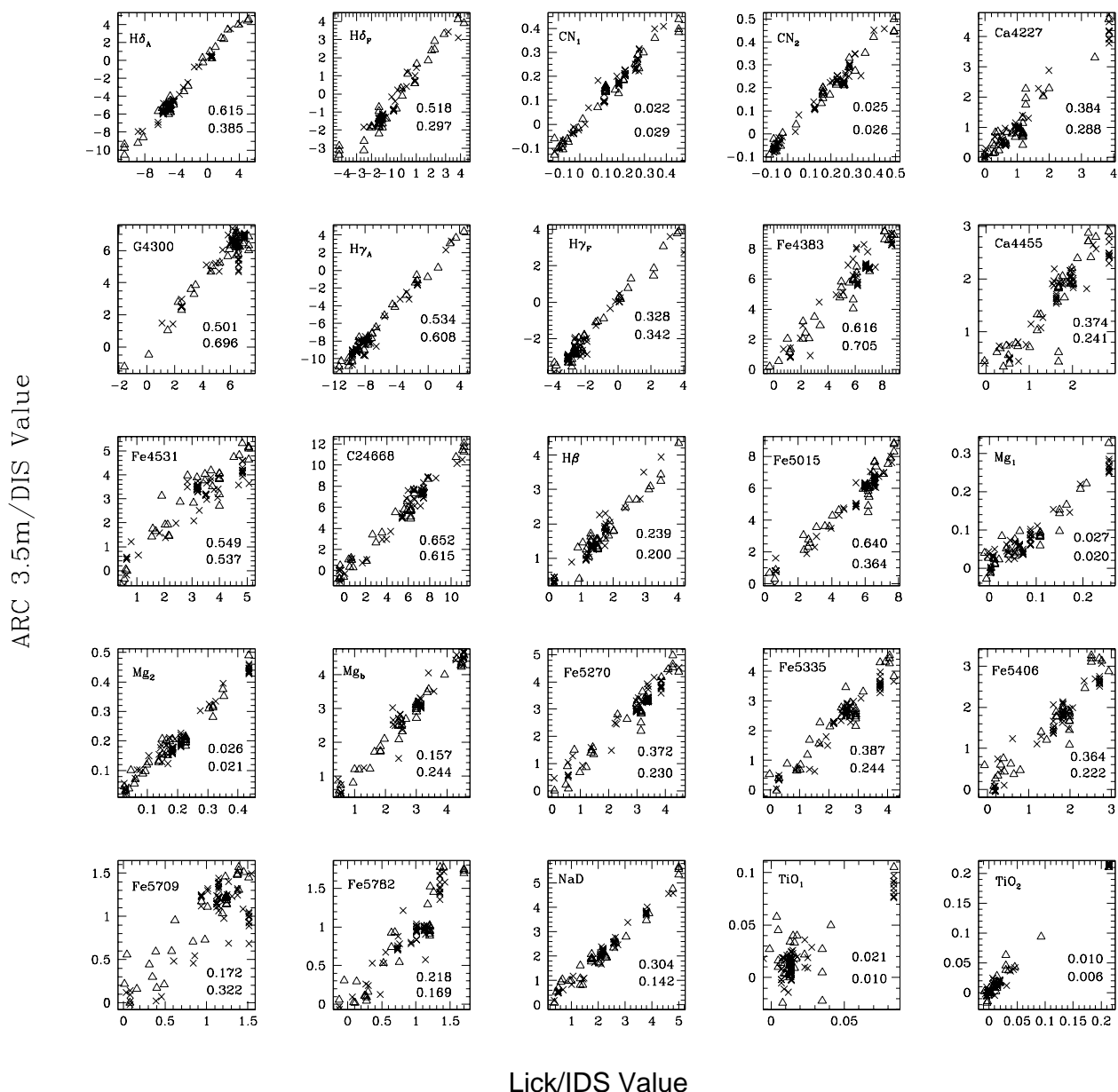


Figure 2. Transformations to the Lick/IDS system. Each point is a Lick standard star. Triangles are DIS I. Crosses are DIS III. DIS III transformation were used for DIS II. The rms scatter when applying the transformations on the stars are shown at the bottom-right of each plot (with DIS I above DIS III).

between this work, long-slit data from Fisher et al. (1996; crosses), IFU data from Sil'chenko et al. (2003; asterisks), and SAURON data from de Zeeuw et al. (2002; squares) for NGC 3384. Here also, Sil'chenko's profile is averaged azimuthally while de Zeeuw et al.'s is an extraction along the major axis. This galaxy was observed on the night in which scattered light was corrected for as described in Section 3.2. Fisher et al.'s profiles are in good agreement with those from SAURON. Our Mg_b and Fe5270 profiles agree marginally with published values. In the central regions, our $H\beta$ profile

falls in between de Zeeuw et al.'s and Sil'chenko et al.'s. Outside about 15 arcsec, our profile falls steeply, possibly due to inadequate scattered light correction, while de Zeeuw et al.'s stays flat. Our Fe5335 profile is much steeper than the published ones especially outside 15 arcsec (again likely due to inadequate scattered light correction). Two of the index-combinations studied in this paper, $[MgFe]'$ and $Mg_b/\langle Fe \rangle$, include Fe5335. The discrepancy between our Fe5335 profile NGC 3384 and published ones does not affect $[MgFe]'$ significantly. Fisher et al.'s profile (cyan curve in Fig. 8) shows

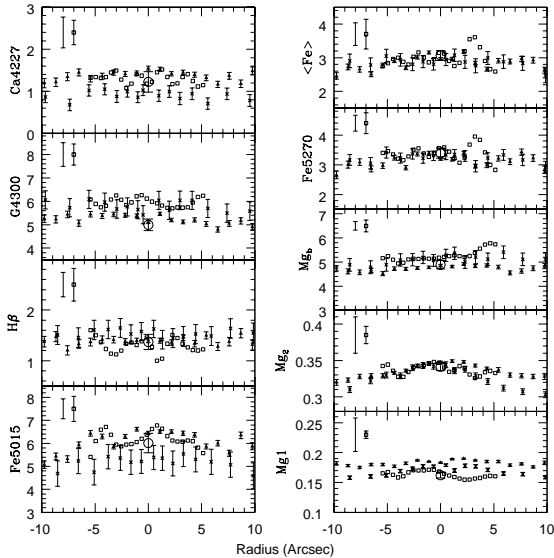


Figure 3. Comparison of line strength gradients between this work and published values for NGC 4472. Triangles are from this work. Large circles are from Trager et al. (1998). Open squares are IFU data from Peletier et al. (1999) and crosses are long-slit data from Vazdekis et al. (1997). At the top of each figure, error bars without points represent the scatter in stars from our transformations to the Lick system; error bars with squares indicate uncertainties in Peletier et al.’s data, including those involved in transforming to the Lick system.

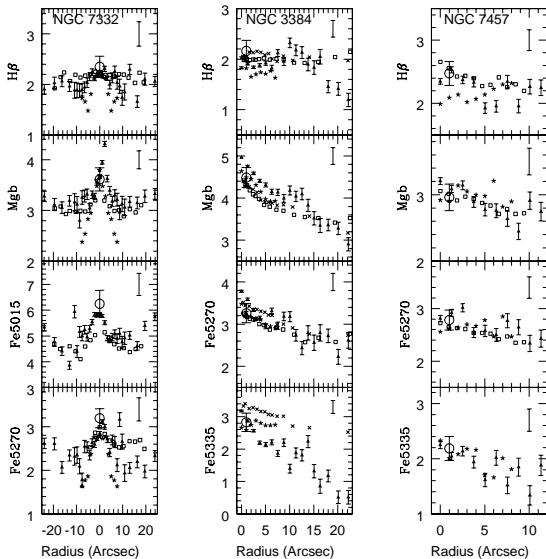


Figure 4. Comparison of line strength gradients between this work and published values for NGCs 7332, 3384, and 7457. Triangles are from this work. Asterisks are azimuthally averaged IFU data from Sil’chenko (1999), Sil’chenko et al. (2003), and Sil’chenko et al. (2002) for NGCs 7332, 3384, and 7457 respectively. Squares are SAURON data extracted along the major-axis from Falcón-Barroso et al. (2004), de Zeeuw et al. (2002), and Sil’chenko et al. (2002). For NGC 3384, crosses are long-slit data from Fisher et al. (1996).

good agreement with ours. For $Mgb/\langle Fe \rangle$ however, we obtain a positive gradient while Fisher et al. found no gradient (Fig. 16), possibly due to scattered light in our data. The other two objects affected by scattered light are NGCs 2787 and 3945. NGC 2787 shows no gradient in $Mgb/\langle Fe \rangle$. NGC 3945 has an asymmetric positive gradient. This could not be due entirely to scattered light since the scattered profile was symmetric.

The third column of Fig. 4 compares profiles for NGC 7457 with IFU data from Sil’chenko et al. (2002) and archival SAURON data which were also presented in Silchenko et al.’s paper. Silchenko et al.’s values are systematically smaller in the central regions than those obtained by others except for the case of Fe5335, where they are in agreement with ours. Our values have larger scatter but are otherwise in agreement with the SAURON values. The agreement among studies is worst for $H\beta$ although this galaxy has little or no Balmer emission. The 2D SAURON map shows a negative gradient along the major axis but not along the minor axis while Sil’chenko et al.’s 2D map shows no gradients whatsoever; our values are in better agreement with SAURON’s than Sil’chenko et al.’s.

3.7 Absorption Line Indices and SSP Models

We have measured all 25 Lick indices in our galaxies as a function of galactocentric radius. In this paper, we concentrate on a subset of these indices which are sensitive to age, metallicity, and α/Fe . The most age-sensitive indices are the Balmer indices $H\beta$, $H\gamma_A$, $H\gamma_F$, $H\delta_A$, and $H\delta_F$. Of these, $H\beta$ suffers most from line-filling by emission while the $H\delta$ indices are the least affected. On the other hand, $H\beta$ offers the most orthogonality with respect to metallicity-sensitive indices. Using a combination of the Balmer indices, we can obtain more reliable age estimates than with just one index. For metal lines, we compute the indices $Mgb/\langle Fe \rangle$ and $[MgFe]'$ as discussed in TMB; the former is directly related to α/Fe , and $[MgFe]'$ traces metallicity without any sensitivity to α/Fe . Individually, $[MgFe]'$ and the Balmer indices are degenerate in age and metallicity but together they can break the degeneracy since each index has a different age-metallicity dependence.

The integrated-light spectrum of an object is a linear combination of SSPs. Some objects, such as globular clusters, are well represented by a single SSP while galaxies are generally not. Still, one can characterize the SPs of a galaxy by an “equivalent SSP”. Since the integrated light from a galaxy is weighted by luminosity, its SSP age and metallicity is likely to be different from the mass-weighted age and metallicity of its stars. SSP values are useful parameterizations of the SPs but cannot be interpreted as true ages and metallicities, since galaxies most likely contain a range of both. To avoid over-interpreting our data, we focus on the line strengths, mentioning SSP values only to illustrate dramatic differences between objects or regions within an object (i.e. 2 vs 10 Gyr as opposed to 8 versus 12 Gyr). Different line strengths in different objects (or within an object) imply different SPs; the SSP models allow us to infer the underlying source of the differences.

3.8 Bulge-to-disk decomposition

One-dimensional and two-dimensional bulge-to-disk decomposition (B/D) was performed on our images. The disk and bulge were simultaneously fit with an exponential and an $\exp[r^{1/n}]$ profile, respectively. Initial fits were made using fixed n of 1, 2, 3, and 4; the best fit of these was used as a starting guess in a final fit where n was allowed to vary as a free parameter. The results from the 1D decomposition were used as starting guesses for the 2D. In the 2D fits, both the bulge and disk components were allowed to be elliptical. This resulted in bars being fit as bulges in some galaxies (IC 302 and NGCs 266, 765, 3681, 3883, 5375) but not others (IC 267 and NGCs 2487 and 5020). A two-component bulge/disk model, such as ours, also overestimates the bulge component of our three S0s with luminous inner disks (NGCs 2787, 3384, and 3945) as previously found by Erwin et al. (2003). We pay close attention to these effects when studying the line strength profiles in the bulge- and disk-dominated regions (Section 4.2). It was found through visual inspection that the best-fitting bulge and disk components of the other galaxies were reasonable. Fig. 5 shows the light profiles of our galaxies along with the best-fit bulge and disk components.

The bulge-to-disk decomposition used here primarily serves to determine the relative contribution of bulge and disk light as a function of radius; while B/D decomposition is notoriously difficult, especially when allowing for a Sersic bulge, this ratio is determined more robustly than the derived values of bulge effective radius and Sersic index.

Throughout this paper, the term “disk” refers to the exponential outer region of the luminosity profile and the term “bulge” refers to the excess light in the inner regions that was fit with a Sersic profile. It is possible that these photometrically-determined components do not correspond to a cold and a hot component, a flat and a spheroidal component, or a young and an old component. Through simulations, Abadi et al. (2003) found that while the stars of a simulated galaxy were well fit by a Sersic + exponential profile, the hot and cold components were not well fit individually by a Sersic and an exponential profile respectively. Instead both were Sersic in the inner regions and exponential further out. Using our kinematic information, we address this issue in Paper II. The structural properties and how they relate to the SPs will also be presented in that paper.

4 RESULTS

4.1 Central Line Strengths

Fig. 6 shows the measured central values of $H\beta$ and $[MgFe]'$ for our sample as well as published values for the Milky Way (Puzia et al. 2002), M31 (Puzia et al. 2005), other bulges (Proctor & Sansom 2002) and elliptical galaxies (Trager et al. 1998; Proctor & Sansom 2002). Our central indices were measured on spectral extractions binned to match Trager et al.’s 4 arcsec aperture and Proctor et al.’s 3.6 arcsec aperture as closely as possible (3.3, 4.2, and 3.8 arcsec for DIS I, II, and III respectively). Symbols are as in Fig. 1. Larger symbols denote larger central velocity dispersions. If a point has an accompanying vertical line segment, its location was determined using an average of the other

four Balmer indices instead of $H\beta$ to compute the SSP age. The other end of the line segment shows the $H\beta$ value. If the difference between these is large, this is due most likely to errors in $H\beta$ emission correction since the galaxies whose $H\beta$ values lie outside the model grid have strong $H\beta$ emission. Two galaxies have $H\beta$ values that put them outside the plot range. These are NGCs 2787 and 5719 with $H\beta$ values of -0.506 and 0.607 respectively.

Bulges can be divided into three groups according to which region of Fig. 6 they populate: the old metal-rich (OMR, lower right) region, the young metal-rich (YMR, upper right) region with ages less than 3 Gyr and super-solar metallicity, or the metal-poor (MP, left) region with sub-solar metallicity. This classification scheme is analogous to that of Prugniel et al. with our MP, OMR, and YMR classes corresponding to their A, B, and C classes respectively. Membership in a region is closely related to bulge color. Most of the red bulges populate the OMR region while all but one of the bulges in the MP region are blue. The exception is IC 267 (the red filled square with $[MgFe]'=1.65$). This bulge has strong Balmer emission which suggests that its red color is due to dust from recent star formation as opposed to an old SP. Hereafter, when we discuss blue bulges, we include IC 267 since it is similar, in most respects, to blue bulges and since its B-K color puts it right on the borderline between blue and red classes anyway. Color does not uniquely represent the SPs of blue bulges; some bulges are blue because they are metal-poor while others are blue because they are young. To distinguish the two classes of blue bulges in subsequent plots, the MP bulges are marked with an additional blue dot.

Central line strengths are also sensitive to Hubble type. All the early-type (S0-Sab) bulges have large central metallicities. The blue early-types are in the YMR region while the red early-types are in the OMR region. Bulges of late-type spirals are more heterogeneous in their central line strengths than those of early-types. The MP region is populated exclusively by late-types but late-types are also found in the other two regions. Trager et al.’s ellipticals mostly populate the OMR region with a couple of them lying in the YMR region. Lower-luminosity ellipticals span a similar range of SSP values as our blue bulges (Caldwell et al. 2003); unfortunately, we cannot include Caldwell et al.’s data in Fig. 6 because they did not measure the same indices. The bulges of the MW and M31 lie in the MP region.

Much of the variation in central line strengths is due to correlations between the line strengths and the global kinematics. The different types of bulges (MP, YMR, and OMR) and ellipticals form a continuous and overlapping sequence on a plot of $[MgFe]'$ versus central velocity dispersion (Fig. 7, top-left). In both bulges and ellipticals, $[MgFe]'$ is correlated with σ_0 at the low- σ_0 end. As σ_0 increases beyond $\log \sigma_0 > 2.2$, $[MgFe]'$ remains constant. Bulges show larger scatter than ellipticals in the $[MgFe]'$ - σ_0 relation.

The apparent dichotomy seen in Fig. 6 between the MP bulges and the other objects (namely that the MP bulges have smaller central $[MgFe]'$) is naturally explained by the wide range of σ_0 and V_{max} values spanned by the different types of objects. The MP bulges reside in considerably shallower potential wells than the bulges and ellipticals which populate the OMR and YMR regions. It is important to note here that the predomi-

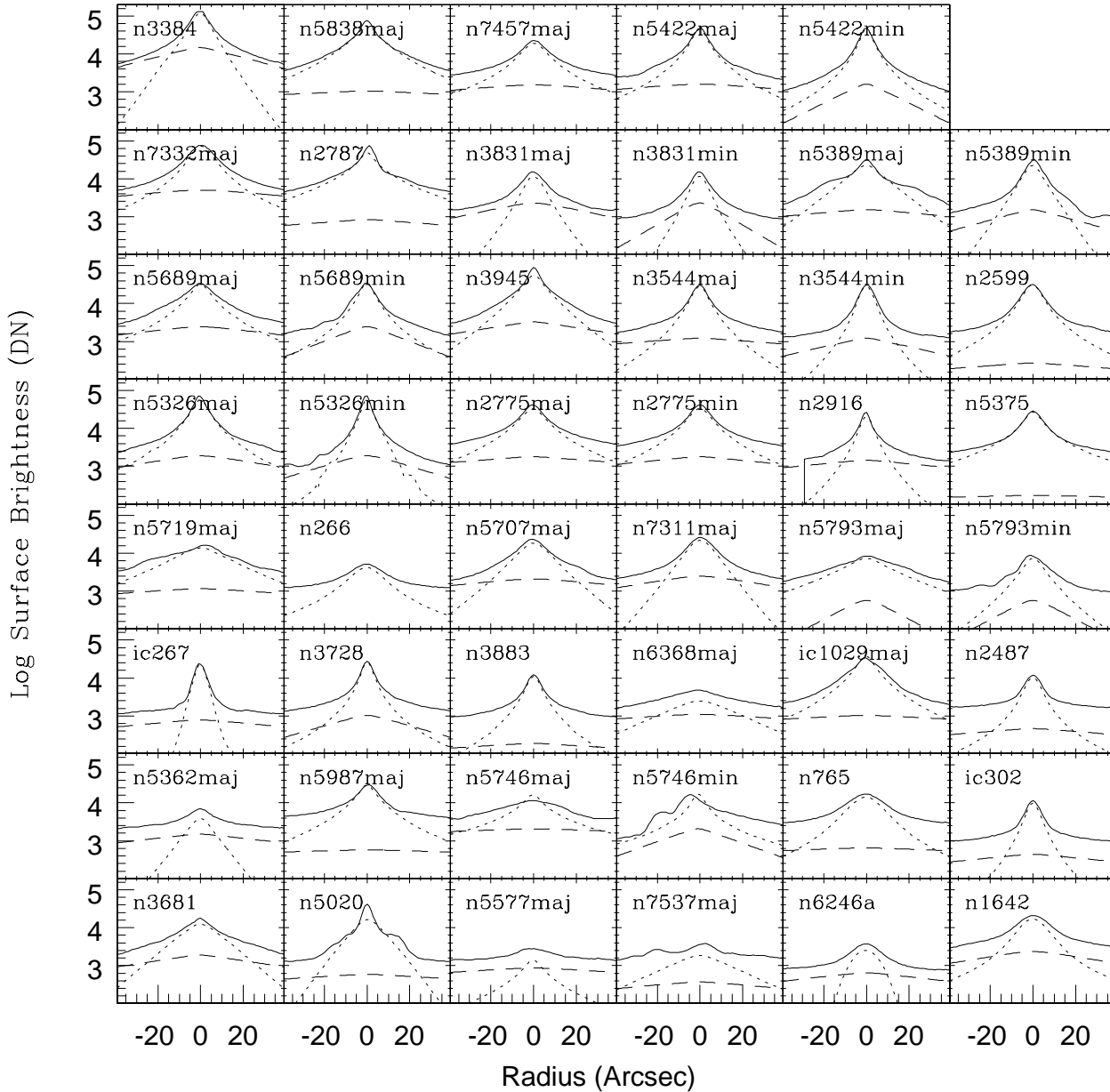


Figure 5. Results of 2D bulge-to-disk decomposition. The light profile of each galaxy is shown as a solid line, the best-fit bulge as a dotted line, and the best-fit disk as a dashed line. The position angles are the same as those used for the spectroscopy (Table 3).

nant view that ellipticals are metal-rich (Trager et al. 2000a; Eisenstein, Hogg, Fukugita, Nakamura, Bernardi, Finkbeiner, 2003; Denicoló et al. 2005; Thomas et al. 2005) applies only to high- σ_0 ellipticals. All of Trager et al.’s ellipticals have $\sigma_0 > 100 \text{ km s}^{-1}$. The three ellipticals from Trager et al’ with the smallest velocity dispersions ($100 < \sigma_0 < 105 \text{ km s}^{-1}$) include the two with the smallest SSP metallicity and the one with the smallest SSP age. Caldwell et al. (2003) found that ellipticals with $\sigma_0 < 100 \text{ km s}^{-1}$ span a similar range of SSP ages and metallicities as our blue bulges.

[MgFe]’ is also correlated with the maximum disk ro-

tational velocity (Fig. 7, top-right), as previously found by Schlegel, Brinkman, and Connolly (1996), and by Ivezić et al. (2002). Significant outliers in the [MgFe]’- V_{max} , having smaller central values of [MgFe]’ than their red counterparts.

Balmer indices are anti-correlated with σ_0 and weakly anti-correlated with V_{max} (middle panel of Fig. 7). Residuals in the $H\beta-\sigma_0$ and $H\beta-V_{max}$ relations are correlated with color such that at a given σ_0 and V_{max} , blue bulges (both MP and YMR) have larger $H\beta$ values than red bulges.

While individual indices are degenerate in age and metallicity, the different symbol sizes in Fig. 6 allow us

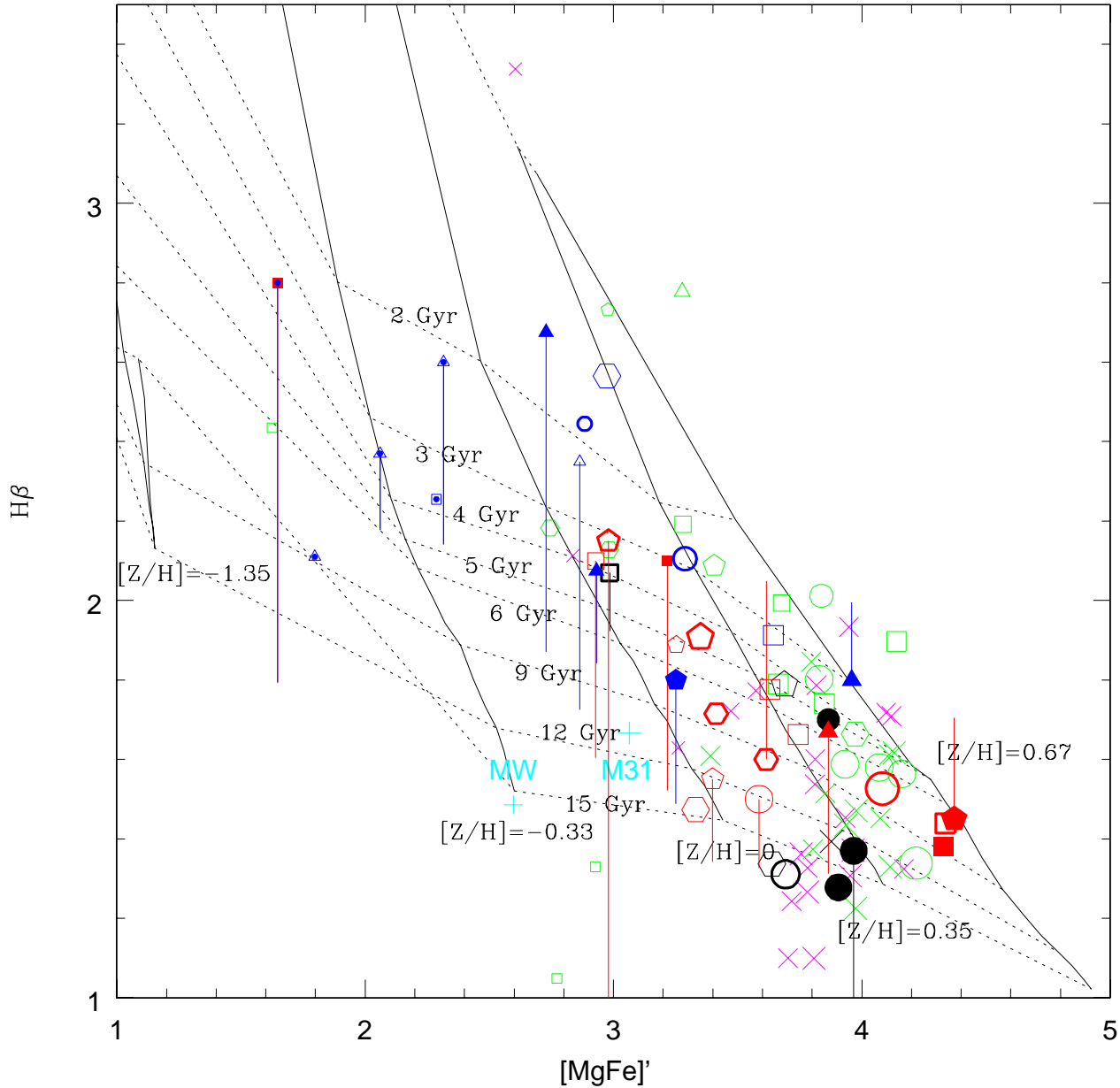


Figure 6. $H\beta$ versus $[MgFe]'$ in the central regions of bulges and ellipticals. Magenta crosses are galaxies from Trager et al. (1998) that were classified as elliptical and had $H\beta$ uncertainty less than 0.2 and velocity dispersion uncertainty less than or equal to 10 km s^{-1} . Green symbols are bulges and ellipticals from Proctor & Sansom (2002). The Milky Way (Puzia et al. 2002) and M31 (Puzia et al. 2005) are shown as '+' symbols. Symbols for our bulges and those of Proctor et al. are as in Fig. 1. Larger symbol sizes were used for objects with larger central velocity dispersion. Bulges for which we do not have color information are in black. The metal-poor (MP) bulges are marked with an additional blue dot. Where spectra exist along both minor and major axes, the average of the two values was used. If a point has an accompanying vertical line segment, its location was determined using an average of the other four Balmer indices, instead of $H\beta$, to compute the SSP age. The other end of the line segment shows the $H\beta$ value. TMB's models are superimposed on the plot.

to determine how metallicity and age vary with σ_0 . Mean SSP metallicity and SSP age are larger in larger- σ_0 galaxies but at fixed σ_0 the scatter in SSP metallicity and SSP age are large. At fixed σ_0 , age and metallicity are known to be anti-correlated in ellipticals (Trager et al. 2000b; Proctor & Sansom 2002). The ellipticals from Trager et al.

with large SSP age have smaller SSP metallicity than those with small SSP age. Such an anticorrelation appears to exist for red bulges but with considerably larger scatter. Interestingly, the small- σ_0 blue bulges also appear to have an age-metallicity anticorrelation.

In bulges and ellipticals, the α/Fe ratio as indicated by

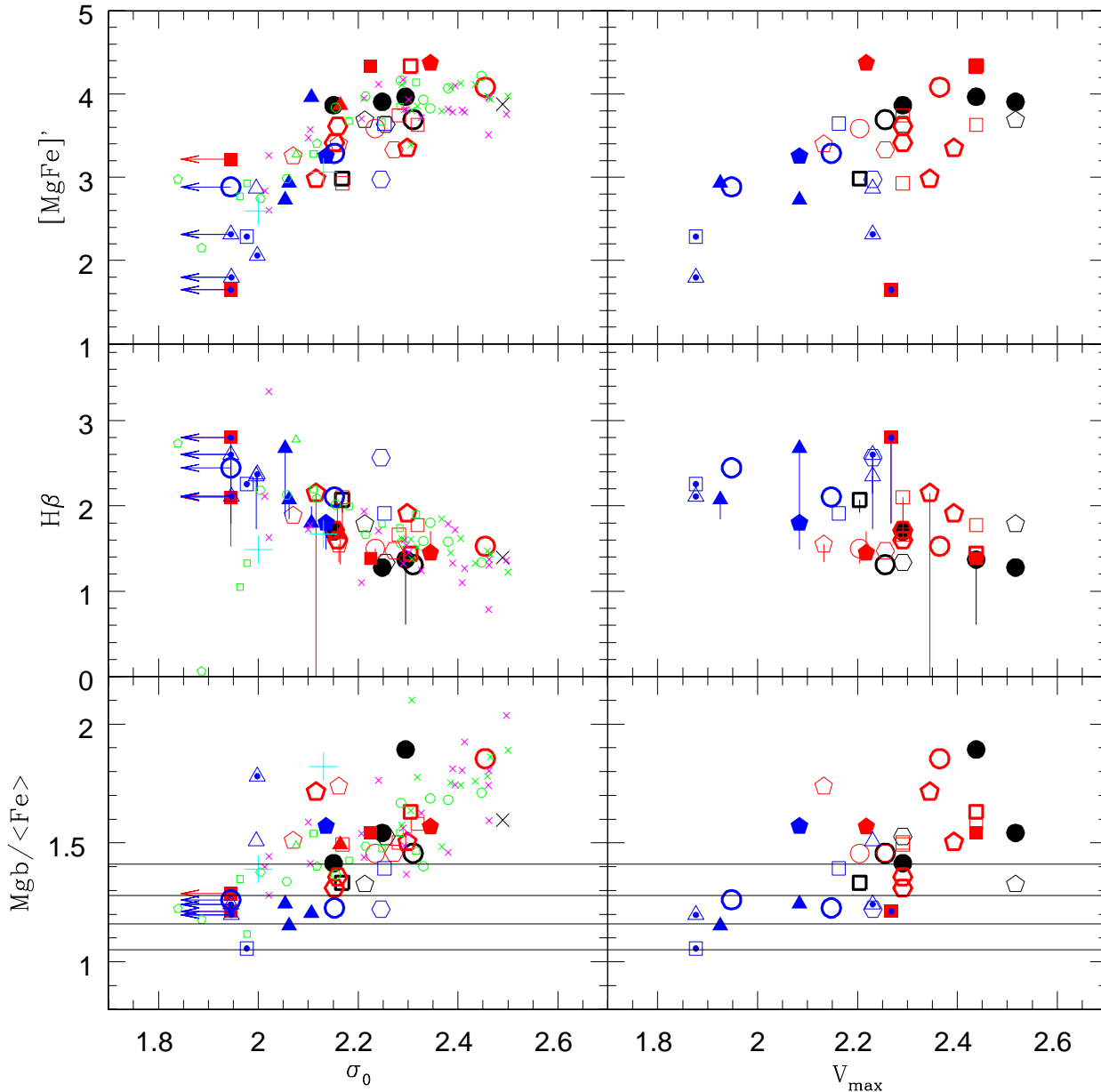


Figure 7. Central line strengths versus central velocity dispersion and maximum disk rotational velocity. Symbols as are in Fig. 6. Arrows represent upper limits for galaxies whose velocity dispersions are close to or below our resolution limit. IC 302 and NGCs 765, 2487, 2916, and 6246A are not shown on the right panel since their inclinations are too low to measure rotation. In the bottom panel, the region within the inner horizontal lines corresponds to models with solar α/Fe for metallicities $-1.35 \leq [Z/H] \leq 0.35$ and ages from 8 to 15 Gyr (from Fig. 4 of TMB). The region within the outer horizontal lines represents models with the same metallicities and ages from 3 to 15 Gyr.

$Mgb/\langle Fe \rangle$, is correlated with σ_0 and V_{max} (bottom panel of Fig. 7). In these two plots, the region within the inner horizontal lines corresponds to models with solar α/Fe for metallicities $-1.35 \leq [Z/H] \leq 0.35$ and ages from 8 to 15 Gyr; the region within the outer lines represents models with the same metallicities and ages from 3 to 15 Gyr (from Fig. 4 of TMB). Red bulges and ellipticals show good overlap in the $Mgb/\langle Fe \rangle$ - σ_0 diagram. With a few exceptions, blue bulges

are consistent with having solar α/Fe . Consequently, most blue bulges have smaller $Mgb/\langle Fe \rangle$ ratios than red bulges or ellipticals at a given value of σ_0 or V_{max} . One of the blue bulges, NGC 6246A, has super-solar α/Fe , large age, and small metallicity ($[Z/H] \sim -0.8$) like MW halo stars. The other two blue bulges with super-solar α/Fe have super-solar metallicity like the majority of red bulges.

There are hints that barred galaxies follow different

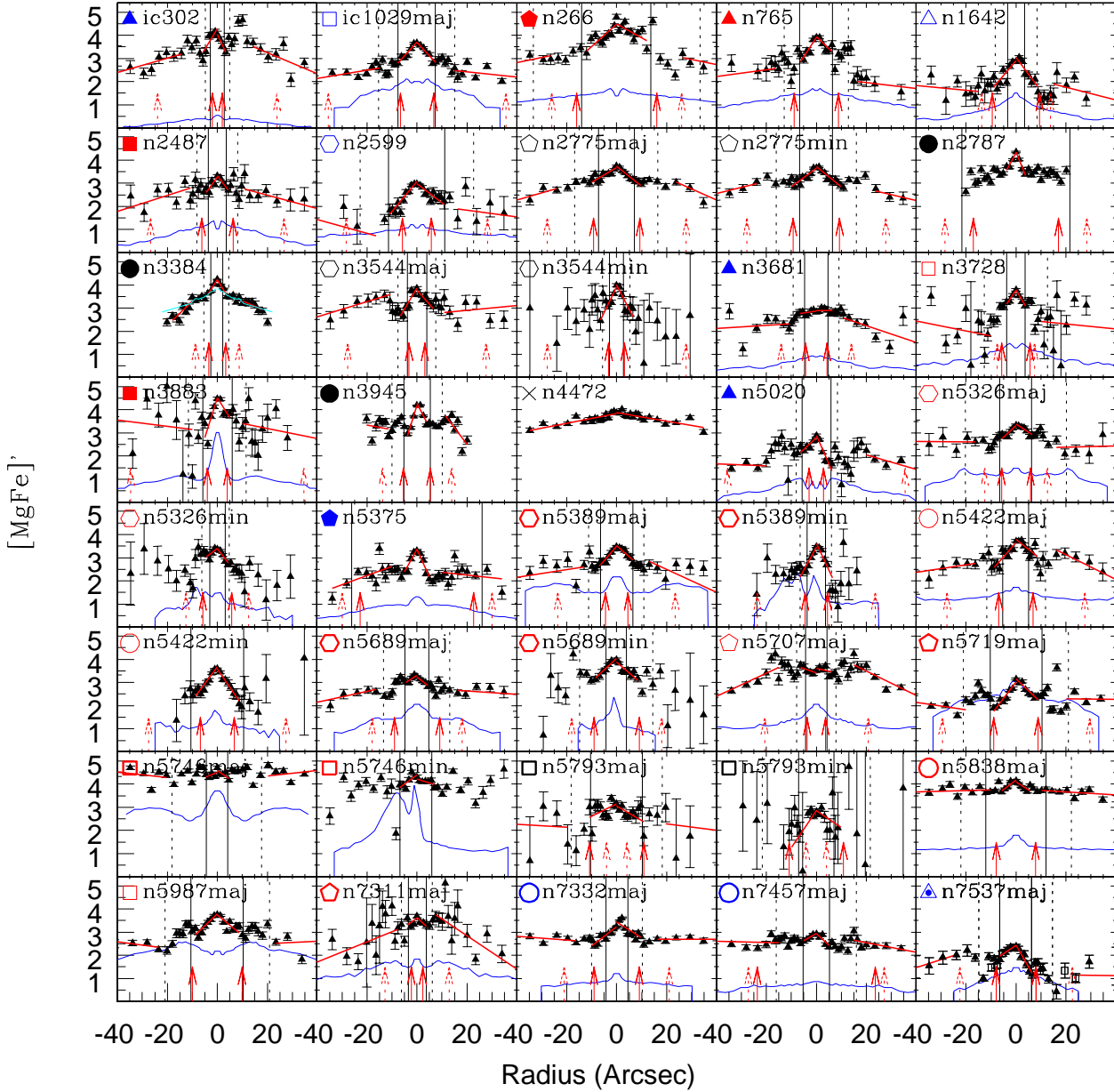


Figure 8. $[MgFe]'$ profiles in our large-bulge galaxies. Open squares and filled triangles show points that were and were not corrected for [NI] 5199 emission respectively. For NGC 3384, the cyan curve shows the profile obtained by Fisher et al. (1996). At the top-left of each plot are symbols denoting the galaxy type (as in Fig. 6) as well as the NGC or IC identifiers. The solid and dotted vertical lines indicate where the ratio of bulge to disk light is two and half respectively, as determined from the bulge-to-disk decomposition. The solid and dotted red arrows indicate the location of the bulge effective radius and disk scale length respectively. Results from linear least-squares fits performed separately in the bulge- and disk-dominated regions are shown in red. Blue lines are color profiles (B-K-3) from PB and DJ. B-K was not available for IC 302; V-H-3 is shown instead.

index- σ_0 and index- V_{max} relations than unbarred galaxies. At fixed σ_0 and V_{max} , barred galaxies appear to have larger central values of $[MgFe]'$ than unbarred galaxies (or galaxies with elliptical-shaped bulges) of the same σ_0 or V_{max} , with IC 267 being the most notable exception. B/p bulges generally lie between and exhibit larger scatter than barred and unbarred/elliptical bulges in the $[MgFe]'$ - σ_0 and $[MgFe]'$ -

V_{max} diagrams. The central regions of b/p bulges could be contaminated by the foreground disk resulting in smaller values of $[MgFe]'$ than those of the low-inclination barred galaxies. Barred galaxies appear to have smaller H β than unbarred galaxies at fixed σ_0 but not at fixed V_{max} . For $2.2 > \sigma_0 > 2.35$, barred galaxies appear to have larger values of $Mgb/\langle Fe \rangle$ but the opposite is true for $2 > \sigma_0 > 2.2$.

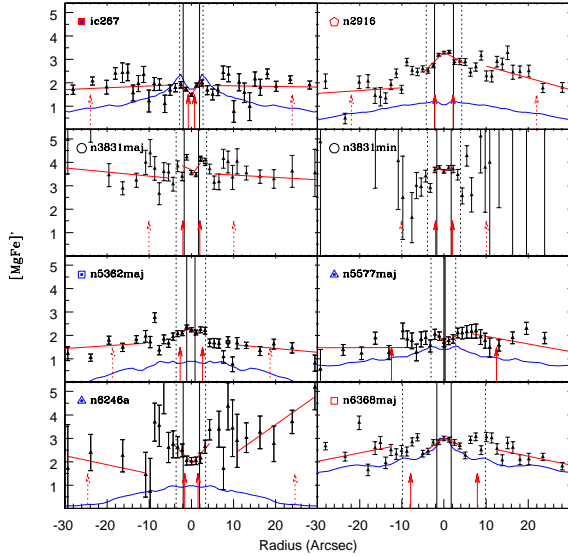


Figure 9. $[\text{MgFe}]'$ profiles in our small-bulge galaxies. Symbols are as in Fig. 6.

No striking difference is seen between barred and unbarred galaxies in the $\text{Mgb}/\langle\text{Fe}\rangle - V_{max}$ relation. These results need to be verified using a large sample of barred and unbarred galaxies as a function of σ_0 and V_{max} .

The central regions of our three barred S0s with disk-like structure and kinematics (filled black circles) have super-solar SSP metallicities and α/Fe ratios and two of the three have large SSP ages. If all disks formed stars on long timescales (several Gyr), we would expect them to have small α/Fe ratios, like the MW disk at the solar neighborhood, since ISM enrichment would eventually be dominated by SN Ia. The “luminous inner disks” of these S0s have not had such a star-formation history. Peletier et al. (1999) found that the Sombrero galaxy is also dominated by a fast rotating disk whose $[\text{Mg}/\text{Fe}]$ is similar not to other disks but to ellipticals of similar mass as the Sombrero.

4.2 Line Strength Gradients

Figs. 8-9 show spatially resolved $[\text{MgFe}]'$ profiles in our galaxies. They are split into two figures according to whether they have large or small bulges. Open squares and filled triangles show points that were and were not corrected for $[\text{NI}] 5199$ emission respectively; the correction was seldom performed. The solid and dotted vertical lines indicate where the ratio of bulge to disk light is two and one half respectively, as determined from the bulge-to-disk decomposition. In the central regions, indices were measured on approximately 1 arcsec bins.

The large-bulge galaxies have five or more measurements within the solid vertical lines while the small bulge galaxies have three or fewer. We performed linear least-squares fits to the $[\text{MgFe}]'$ profiles separately in the bulge- and disk-dominated regions, selecting the points to include based on the bulge-to-disk decomposition but making exceptions where they seemed appropriate (such as when the bar was fit as a bulge; see Section 3.8). We usually avoided the

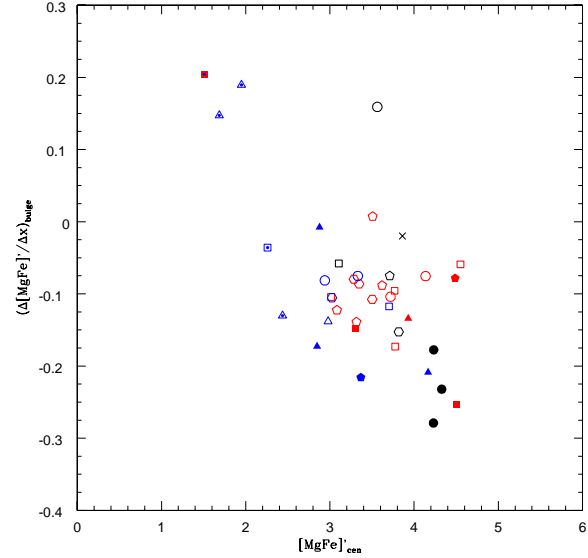


Figure 10. The $[\text{MgFe}]'$ gradient within the bulge-dominated region versus the central value of $[\text{MgFe}]'$. Symbols are as in Fig. 6.

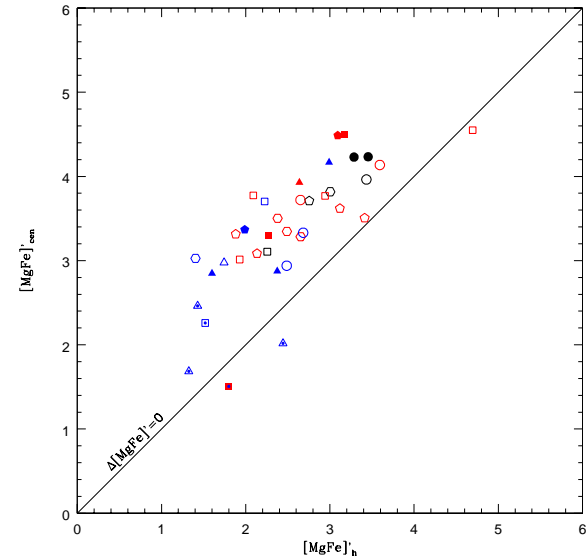


Figure 11. The central value of $[\text{MgFe}]'$ versus the value at one disk scale length computed using the results from a least-squares fits to the $[\text{MgFe}]'$ profiles. The solid line shows where objects would lie if their bulges and disks were identical in $[\text{MgFe}]'$. Symbols are as in Fig. 6.

transition region from bulge to disk dominance. The best-fit lines are shown in red. The large-bulge galaxies have negative $[\text{MgFe}]'$ gradients (weaker $[\text{MgFe}]'$ with increasing radius) in the bulge-dominated region. In all but two of these, $[\text{MgFe}]'$ decreases steadily from the galaxy center to the solid vertical lines, beyond which the slope of the profile changes. The exceptions are NGCs 3681 and 5707, where $[\text{MgFe}]'$ is constant within the solid vertical lines but decreases in the bulge-disk transition. In low-inclination galaxies and along

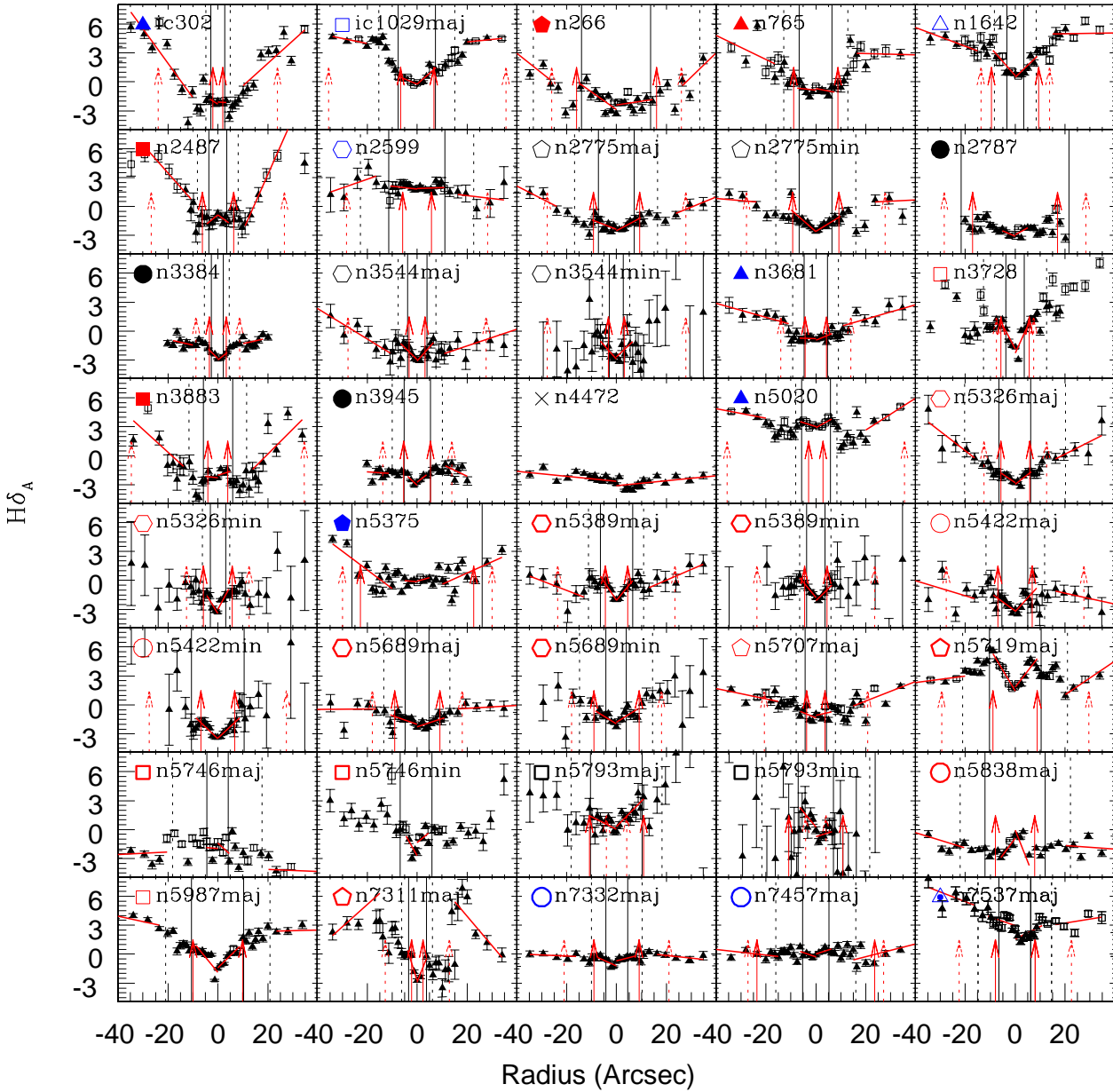


Figure 13. $H\delta_A$ profiles in our large-bulge galaxies. Symbols are as in Fig. 6.

the major axes of inclined galaxies, $[MgFe]'$ is usually larger just outside the solid vertical lines than inside it (NGC 5987 is a good example). The fact that we can identify distinct bulge and disk components in the $[MgFe]'$ profiles suggests that disk contamination is not significant within the solid vertical lines.

Another test for disk contamination is how the major and minor axis profiles vary as a function of inclination. Low-inclination galaxies should have identical profiles if there are no azimuthal differences in line strengths. The major and minor axis profiles of NGC 2775, the only low-inclination galaxy for which both were obtained, are indeed identical.

The minor axis profiles of the edge-on large-bulge galaxies (NGCs 5422, 5689, 5746, 5793) continue decreasing beyond the distance at which the major axis profiles flatten off, a result previously obtained by Fisher et al. (1996) for edge-on S0s. This implies that the outer bulge has lower metallicity than the inner disk. At intermediate inclinations, one expects more disk contamination on one side of the minor axis (the dusty side) than the major axis for the same solid angle. In the three intermediate inclination galaxies for which we have major and minor axis spectra (NGCs 3544, 5326, and 5389), this effect is clearly seen; the profile is asymmetric outside the solid vertical lines with the profile turning over

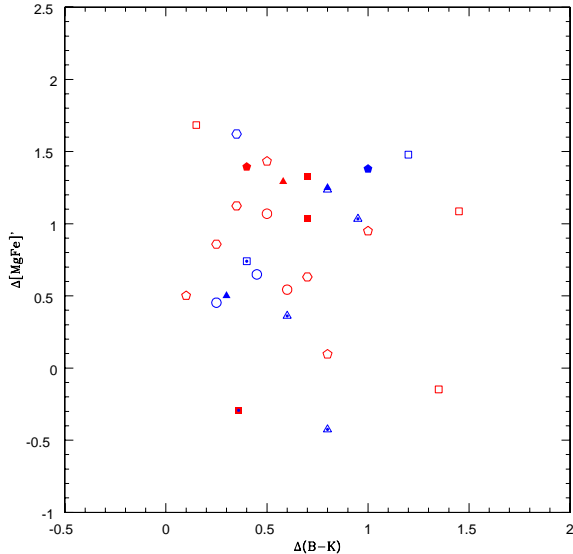


Figure 12. $[\text{MgFe}]'$ gradient versus B-K color gradient, where a gradient is defined as the difference between the value at the center of the galaxy and the value at the disk scale length. Symbols are as in Fig. 6.

at a smaller galactocentric distance on the dusty (left) side than on the dust-free side. Within the solid lines, there is good agreement in gradient slopes between major and minor axes, indicating that disk contamination is not significant.

The small-bulge galaxies generally do not have negative $[\text{MgFe}]'$ gradients within the bulge-dominated region. In four of them (IC 267 and NGCs 3831, 5577, and 6246A), there is the hint of a positive gradient while the rest (NGCs 2916, 5362, and 6368) are consistent with having little or no gradient. Since the profiles are always different inside and outside the solid lines, they cannot be explained by disk contamination.

The slopes of the $[\text{MgFe}]'$ gradients within the bulge are shown in Fig. 10 as a function of the central $[\text{MgFe}]'$ values. Galaxies with large central values have correspondingly large negative gradients while the three galaxies with the smallest central values, namely IC 267 and NGCs 5577 and 6246A, have positive gradients. Since central $[\text{MgFe}]'$ is correlated with σ_0 and V_{max} , it follows that the slope of $[\text{MgFe}]'$ gradients in bulges is correlated with the global kinematics.

Most galaxies also have negative gradients in the disk-dominated region but it is shallower than that of the bulge. Some galaxies (e.g. NGCs 5746, 5838, and 7332) have no gradient in the disk.

The $[\text{MgFe}]'$ value at one disk scale length (computed using the results of our least-squares fits) is correlated with the central value (Fig. 11). This indicates that the metallicity of the disk is correlated with that of the bulge. This correlation holds for all galaxies, not just those with bars, blue bulges, or bulges identified as having disk-like structural or kinematical properties.

The blue lines in Figs. 8-9 are color profiles ($B - K - 2$) from PB and DJ. The shapes of the $[\text{MgFe}]'$ and color profiles agree often but not always. Discrepancies occur most

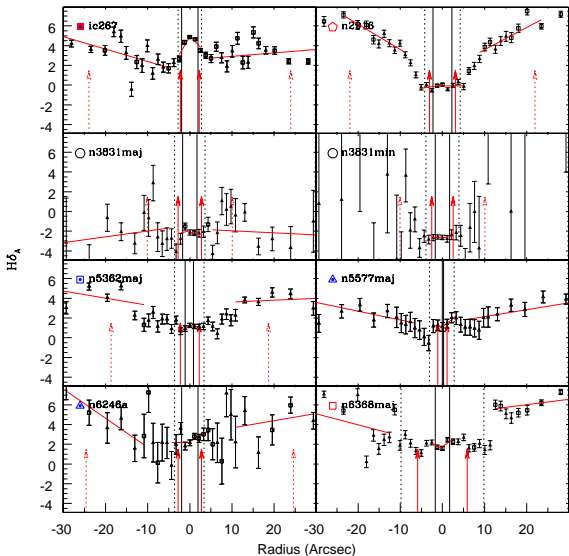


Figure 14. $H\delta_A$ profiles in our small-bulge galaxies. Symbols are as in Fig. 6.

often in the central regions. Several galaxies (e.g. IC 267 and NGC 266, 2487, 2916, 3728, and 5577) show a positive color gradient in the central 5 arcsec; of these, only IC 267 and NGC 5577 have a corresponding positive $[\text{MgFe}]'$ gradient. On the other hand, the central region of NGC 6246A has a positive $[\text{MgFe}]'$ gradient but its color profile is flat. de Jong (1996) noted that it is not possible to identify distinct bulge and disk components using the color profiles. However, it is possible to do so using the $[\text{MgFe}]'$ profiles. As mentioned earlier, the slopes of the $[\text{MgFe}]'$ profiles are almost always distinct inside and outside the bulge-dominated region, with the former usually having a steeper negative gradient. 11 out of the 14 DJ galaxies and 15 out of the 17 PB galaxies have negative $[\text{MgFe}]'$ gradients in the bulge-dominated region. The majority of the PB galaxies (12 out of 17 as opposed to 4 out of the 14 DJ galaxies) also show a negative color gradient in the bulge-dominated region. The systematic difference in color gradients between the PB and DJ samples is likely due to different amounts of extinction at different inclinations since the PB galaxies have large inclinations while the DJ galaxies have small ones.

If we compare the gradient in $[\text{MgFe}]'$ from the galaxy center to the disk scale length (computed using the fit results) with the color gradient (read from the profiles), we find that these two quantities are not tightly correlated (Fig. 12). This is most likely due to the discrepancy between $[\text{MgFe}]'$ and color profiles in the central regions of some galaxies, which in turn is due most likely to the color profiles being affected by dust.

Gadotti & dos Anjos (2001) found a greater prevalence of null or positive color gradients in barred galaxies than in unbarred galaxies. They interpreted their result as evidence for gradients being erased by bar-driven mixing. We do not see any systematic difference between barred and unbarred galaxies with regard to their gradients. Also, if bars homogenized the SPs, we might expect a smooth transition in the line strength profiles from the bulge to the bar. However,

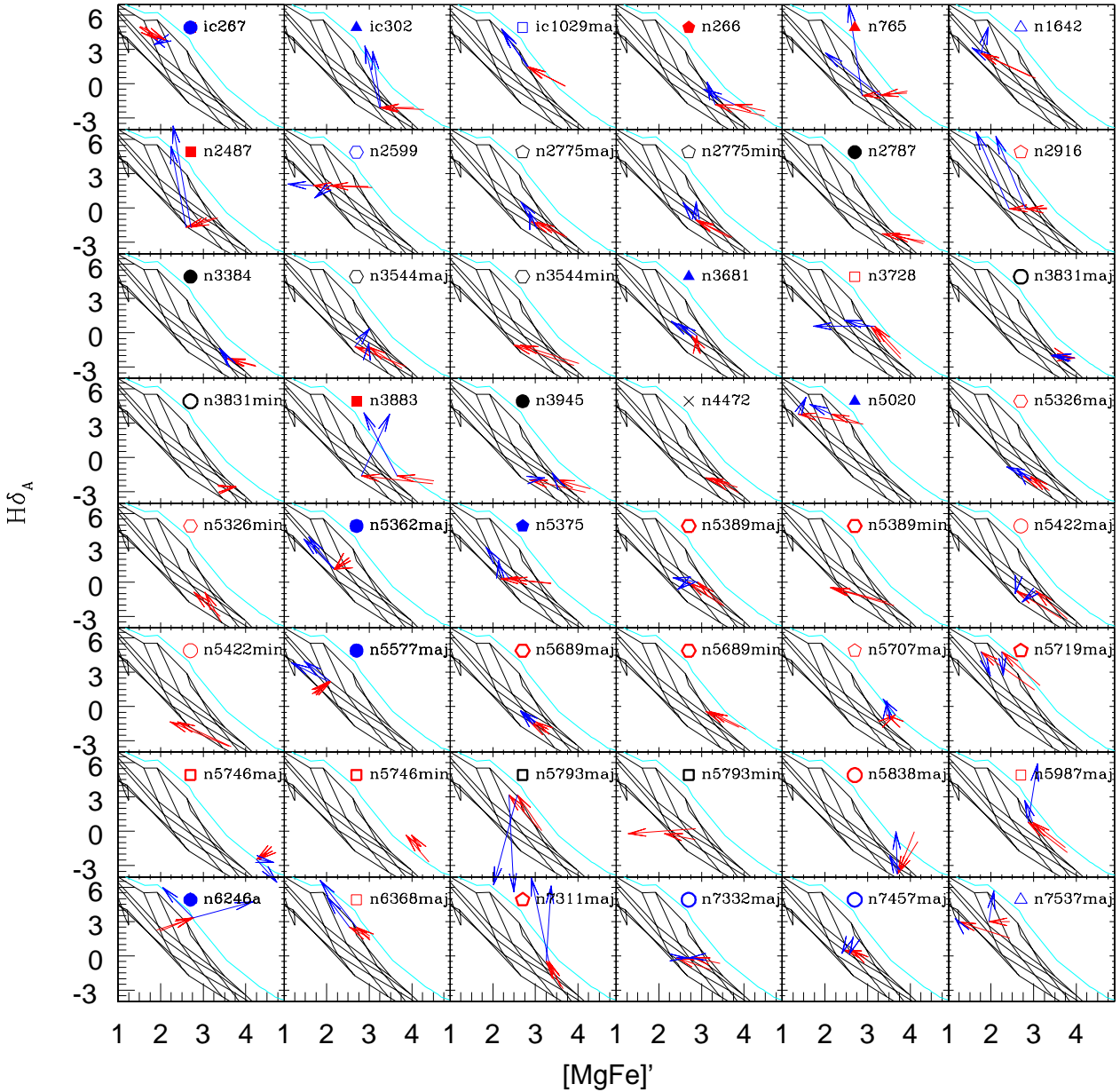


Figure 15. Gradients in $H\delta_A$ and $[MgFe]'$. Red arrows are drawn from the galaxy center to the edge of the bulge-dominated region on either side of the galaxy. Blue arrows are drawn from the edge of the bulge-dominated region to the disk scale length. Symbols are as in Fig. 6. TMB models with solar α/Fe , age=1, 2, 3, 6, and 15 Gyr, and $[Z/H]=-1.35, -0.33, 0, 0.35,$ and 0.67 are overlaid. Unlike $H\beta$, the higher order Balmer indices are not independent of α/Fe . α -enhanced models are parallel to the solar models, lying above and to the right. The cyan curves show models with age=1 Gyr and $[Z/H]=0.67$ for $[\alpha/Fe]=0.3$.

the outer bulges of barred galaxies have lower $[MgFe]'$ than the inner bar the same way the outer bulges of unbarred galaxies have lower $[MgFe]'$ than the inner disk.

4.2.1 Separating Age and Metallicity Effects

Fig. 13 shows gradients in the $H\delta_A$ index. The $H\delta$ profiles show less scatter than the lower-order Balmer indices since they are less affected by emission. Squares and filled tri-

angles show points that were and were not corrected for emission, respectively. Least-squares fits were performed on the Balmer indices exactly in the same manner as for the $[MgFe]'$ profiles. The fit results for $H\delta_A$ are shown in red in Fig. 13. Gradient slopes computed on individual indices were combined to disentangle the effects of age and metallicity. This is shown in Fig. 15 for the $[MgFe]'$ - $H\delta_A$ index combination. A red arrow is drawn from the galaxy center to the edge of the bulge-dominated region (on either side of

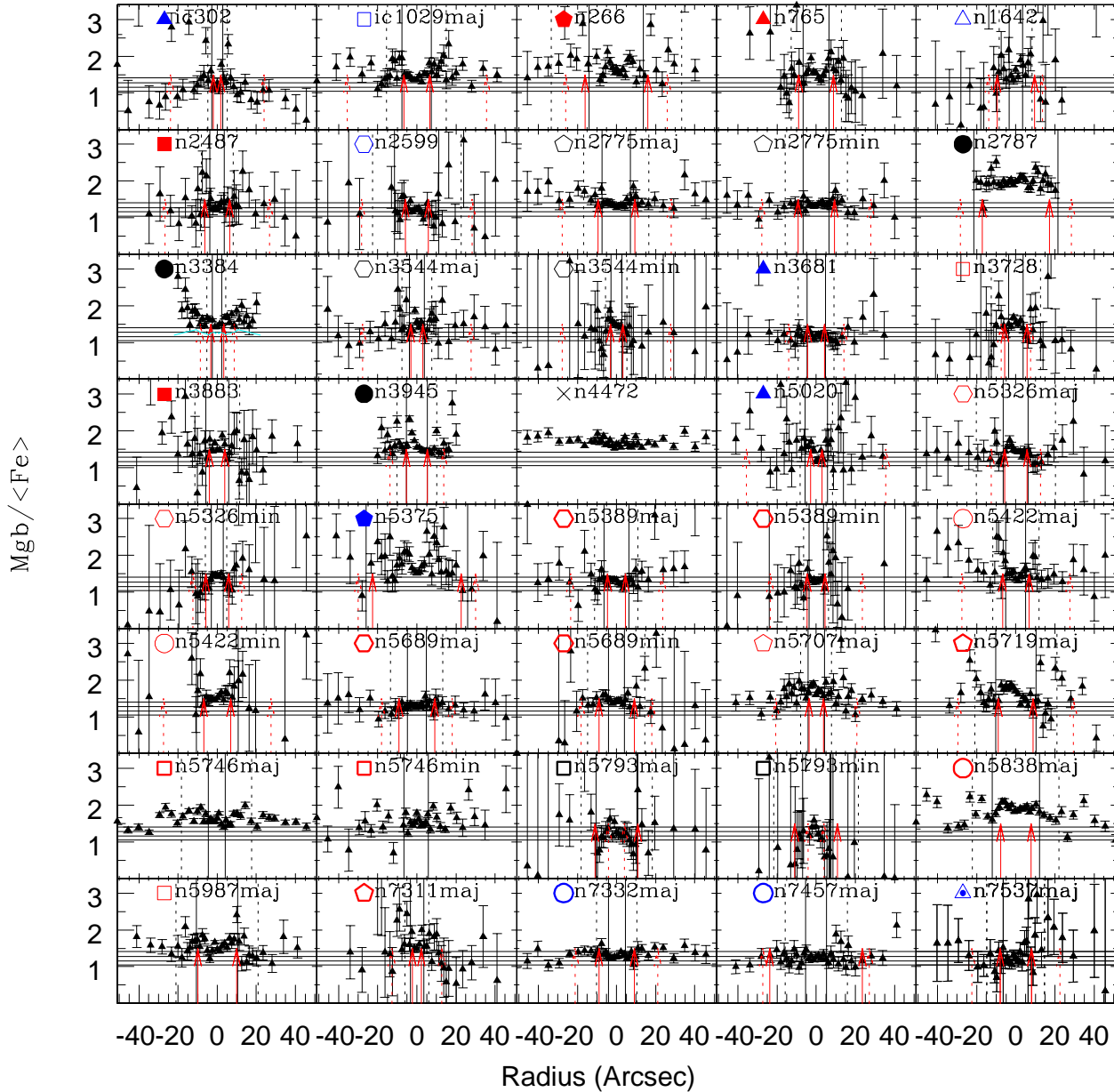


Figure 16. $Mgb/\langle Fe \rangle$ profiles in our small-bulge galaxies. For NGC 3384, the cyan curve shows the profile obtained by Fisher et al. (1996). Symbols are as in Fig. 6. The horizontal lines are as in 7.

the galaxy) and a blue arrow is drawn from there to the disk scale length.

The majority of galaxies (at least 29 out of 38) have negative metallicity gradients in the bulge-dominated region. NGCs 3681, 3831, 5362, 5707, and 7311 show little or no metallicity gradient in the bulge. Three of the five MP bulges (IC 267 and NGC 5577 and 6246A) have positive metallicity gradients. The remaining two galaxies (NGCs 5746 and 5793, both edge-on with b/p bulges) show internal discrepancies in the fit results. Except for its minor axis $H\delta_A$ profile, NGC 5746 is consistent with having little or no

metallicity gradient. The minor axis profiles of NGC 5793 consistently a negative metallicity gradient but the major axis profiles show none.

The majority of galaxies are consistent with having little or no age gradient within the bulge. At least ten galaxies (IC 302 and NGCs 266, 765, 2487, 2599, 2916, 3883, 5020, 5375, and 5838) have a positive age gradient (larger age with increasing radius). Of these, seven are barred and one has a b/p bulge. At least five galaxies (NGCs 3728, 5577, 6246A, 7311, and the major axis of NGC 5793) have a negative age gradient in the bulge.

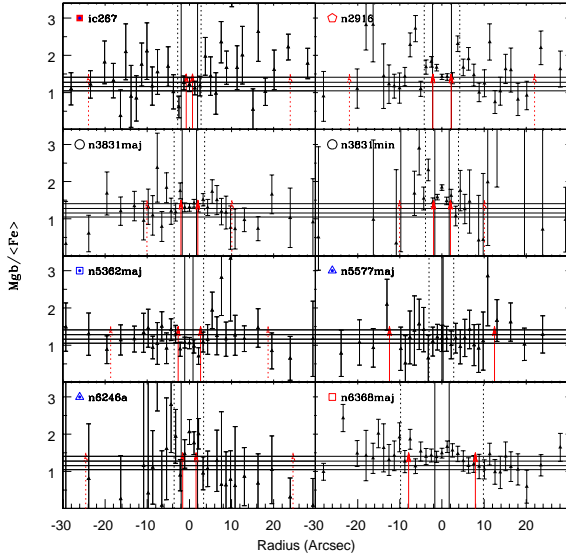


Figure 17. $Mgb/\langle Fe \rangle$ profiles in our small-bulge galaxies. Symbols are as in Fig. 6. The horizontal lines are as in Fig. 7.

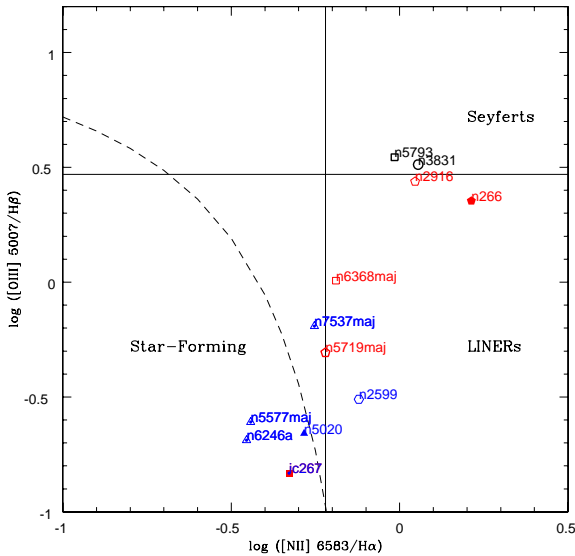


Figure 18. Bulges on the BPT (Baldwin et al. 1981) diagram in which the emission line flux ratio $[OIII]5007/H\beta$ is plotted against the ratio $[NII]6583/H\alpha$. Symbols are as in Fig. 8. The dashed curve shows the demarcation between starburst galaxies and AGN as defined by Kauffmann et al. (2003). We adopt the commonly used definition of LINERs having $[OIII] 5007/H\beta < 3$ and $[NII] 6583/H\alpha > 0.6$ and Seyferts having $[OIII] 5007/H\beta > 3$ and $[NII] 6583/H\alpha > 0.6$.

The Balmer indices show large scatter in the disk-dominated regions, making it difficult to determine whether metallicity and age gradients are present. Plots of gradients in the five Balmer indices versus $[MgFe]$ (such as Fig. 15) do not show consistent results for approximately half the galaxies. Of the other half, most have a negative age gradient and little or no metallicity gradient. Most disks are

solar or sub-solar in metallicity but NGCs 5746 and 5838 are super-solar well into the disk-dominated region.

4.2.2 Abundance Ratio Gradients

Most galaxies either have a positive gradient or no gradient in $Mgb/\langle Fe \rangle$ within the bulge-dominated region (Figs. 16 and 17). The disk-dominated regions generally have solar α/Fe . Since the red-bulge galaxies have super-solar α/Fe in the center, they have a negative gradient in the bulge-disk transition. The blue-bulge galaxies have solar α/Fe in the center. These either have uniformly solar α/Fe or a positive gradient in the bulge and a negative gradient in the bulge-disk transition. Recall that what is marked as the bulge-dominated region in some galaxies (e.g. NGCs 266 and 5375) is actually a bar and that the true bulge-dominated region is smaller. The elliptical galaxy, NGC 4472, is uniformly super-solar in α/Fe .

There are a few galaxies that have super-solar α/Fe in the disk-dominated region. NGCs 266, 5707, and 5746 are nearly uniformly super-solar. The disk of NGC 5838 is super-solar but less enhanced than its bulge.

4.3 Emission Lines in Bulges

Fig. 19 shows profiles of $H\alpha$ and $[NII] 6583$ emission strength in our galaxies. We detect emission in the central regions of all our galaxies except the S0s NGCs 3384 and 7457. The locations of our galaxies on the BPT (Baldwin et al. 1981) diagram of emission line ratios is shown in Fig. 18 for objects with central emission-line EW smaller than -0.5 \AA (the negative sign denotes emission) in $H\alpha$, $[NII] 6583$, $H\beta$, and $[OIII] 5007$. The dashed curve shows the demarcation between starburst galaxies and AGN as defined by Kauffmann et al. (2003). The majority of our emission-line galaxies are AGN. If the emission in these galaxies is due entirely to the AGN, we would expect it to be restricted to the center of the galaxy. However, in the three of these (NGCs 2599, 5719 and 7537), it is not centrally peaked. In the other five (NGCs 266, 2916, 3831, 5793, and 6368), the emission peaks at the center and decreases steadily out to the edge of the bulge-dominated region, beyond which it rises again. Therefore, all or most of the AGN also have active star formation in the bulge-dominated region.

AGN have previously been found to have a larger fraction of young stars than quiescent galaxies (Raimann et al. 2001, 2003). In agreement with these results, we find that most of the AGN have small SSP ages ($< 4 \text{ Gyr}$). The only one with a large SSP age (15 Gyr) is NGC 3831. This could be due to errors from emission correction or from the young component not dominating the total luminosity. Prugniel et al. (2001) found that bulges with emission were small and metal-poor. The star-forming region of our BPT diagram is populated by four blue bulges. They have similar stellar populations as Prugniel et al.'s emission-line galaxies except that one of them (NGC 6246A) has a large SSP age, again possibly due to errors in emission correction.

We see a wide range of behaviors in the emission-line profiles. In some galaxies, such as NGCs 3681 and 5362, there is strong emission in the disk-dominated region but little or no emission in the bulge-dominated region as would

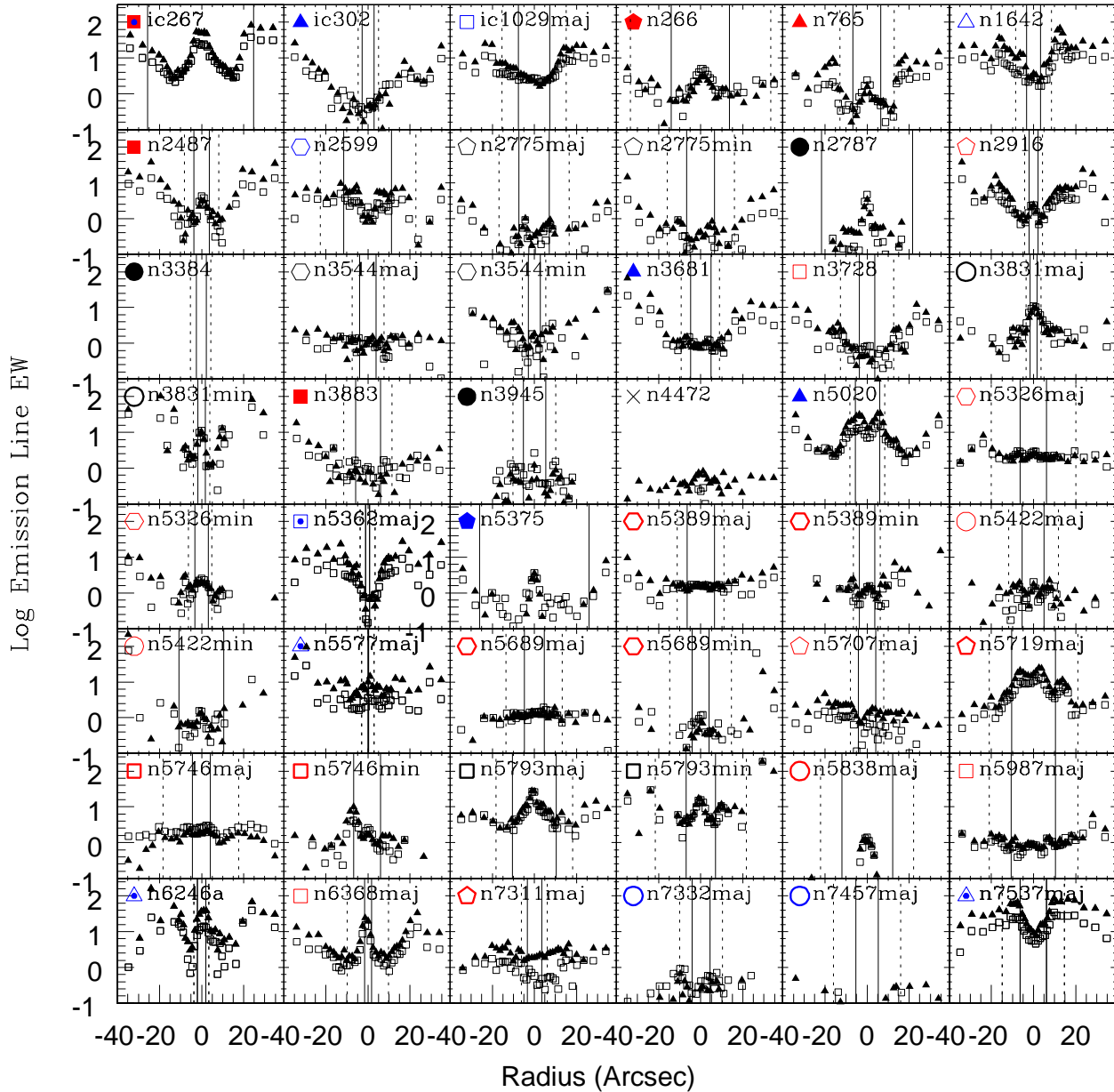


Figure 19. Profiles of emission line strengths in bulges. Triangles are H α . Squares are [NII] 6583. Symbols are as in Fig. 6.

be expected if disks continue to form stars while bulges do not. The only galaxies with little or no emission in the disk-dominated region are S0s. In other cases, there is emission throughout the galaxy but it is weaker in the bulge-dominated region (e.g. NGCs 1642, 2916, 5020, and 7537). This is consistent with a quiescent bulge and a star-forming disk coexisting in the central regions with the ratio of bulge to disk dominance decreasing with radius. Alternatively, the bulge and disk could both be forming stars but the disk more actively so. Finally, in some cases (e.g. IC 267 and NGCs 266 and 5793), the emission lines are strongest at the center.

5 THE FORMATION OF BULGES

As mentioned in the introduction, present-day Λ CDM cosmology argues against the monolithic collapse scenario as does observational evidence for the recent and continuing mass assembly of ellipticals. Of the main proposed formation scenarios, that leaves mergers and secular evolution as possibilities for bulges.

However, the collapse model continues to receive much attention under the claim that it better reproduces the observed line strength profiles of ellipticals. We investigate whether or not this is true for bulges. Gradients in the index Mg_2 have been computed in galaxies formed in col-

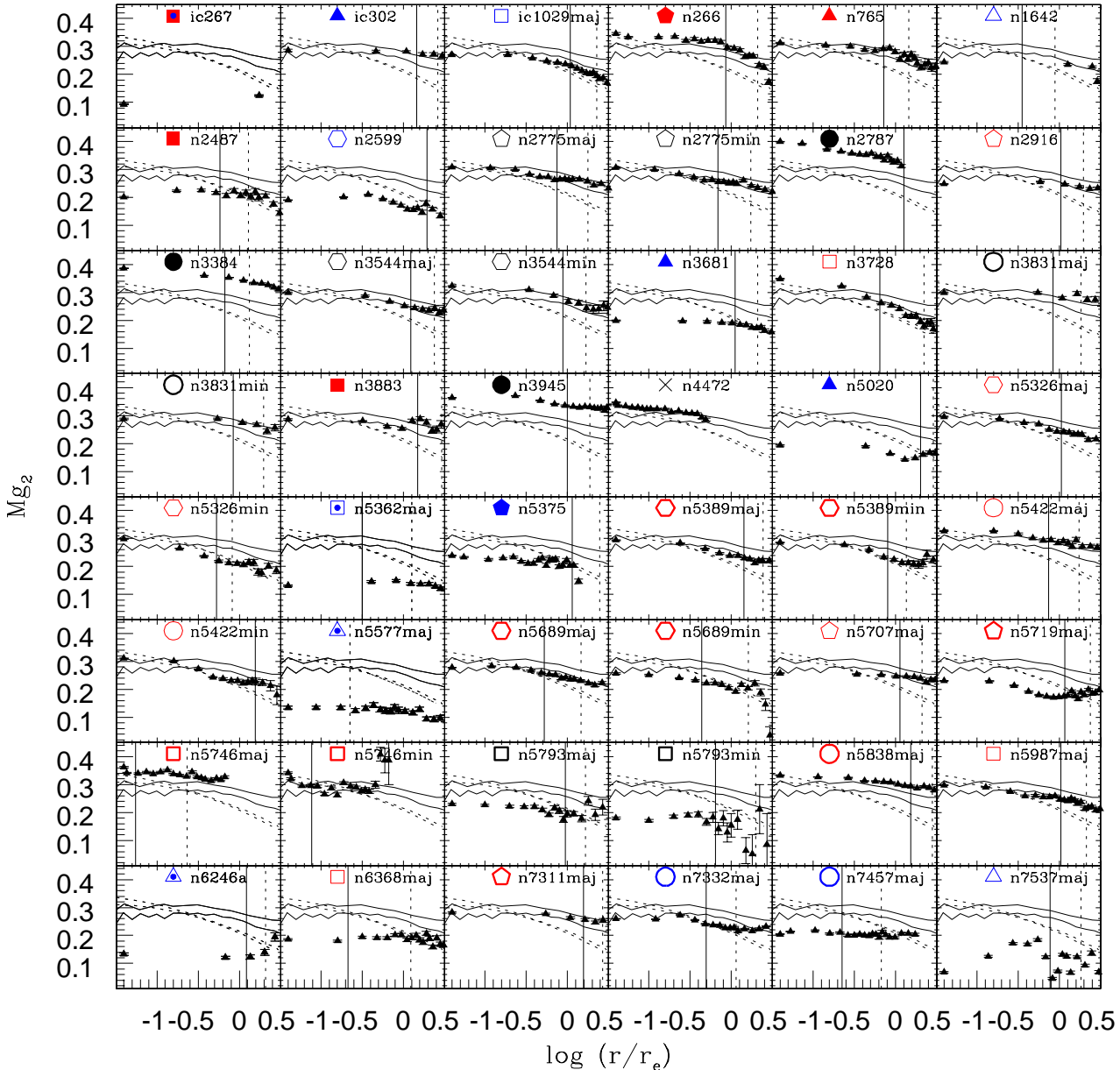


Figure 20. Comparison of Mg_2 profiles between this work and numerical simulations. Solid lines are merger models by Bekki & Shioya (1999) final age 13.1 Gyr and initial disk masses of $10^{10} M_{\odot}$ (bottom curve) and $10^{12} M_{\odot}$. Dotted lines are collapse models by Angeletti & Giannone with final age 13 Gyr (top curve) and 2 Gyr. Symbols are as in Fig. 6.

lapse and merger simulations, allowing for direct comparisons with our data (Figs. 20). Points are our data. Solid lines are two remnants from major disk-disk mergers by Bekki & Shioya (1999) with initial disk masses of $10^{10} M_{\odot}$ (bottom curve in Mg_2 ; top curve in $H\beta$) and $10^{12} M_{\odot}$. The remnants are 13.1 Gyr old. Dotted lines are two collapse models by Angeletti & Giannone (2003) with final ages of 13 Gyr (top curve) and 2 Gyr. We focus on the gradient slopes, assuming that changes in mass and formation epoch mainly shift the models up or down. The collapse models

predict steeper Mg_2 profiles than the merger models. Within the bulge-dominated region, some of our profiles agree with one of the merger models (e.g. NGCs 765 and 7311) while others agree with one of the collapse models (e.g. 3728 and the minor axes of NGCs 5326 and 5422). There are also cases, mostly among blue bulges, where the observed profile is flatter than the merger models (e.g. IC 302). However, the majority of galaxies fall between the collapse and merger models.

Bekki & Shioya also computed $H\beta$ profiles in their mod-

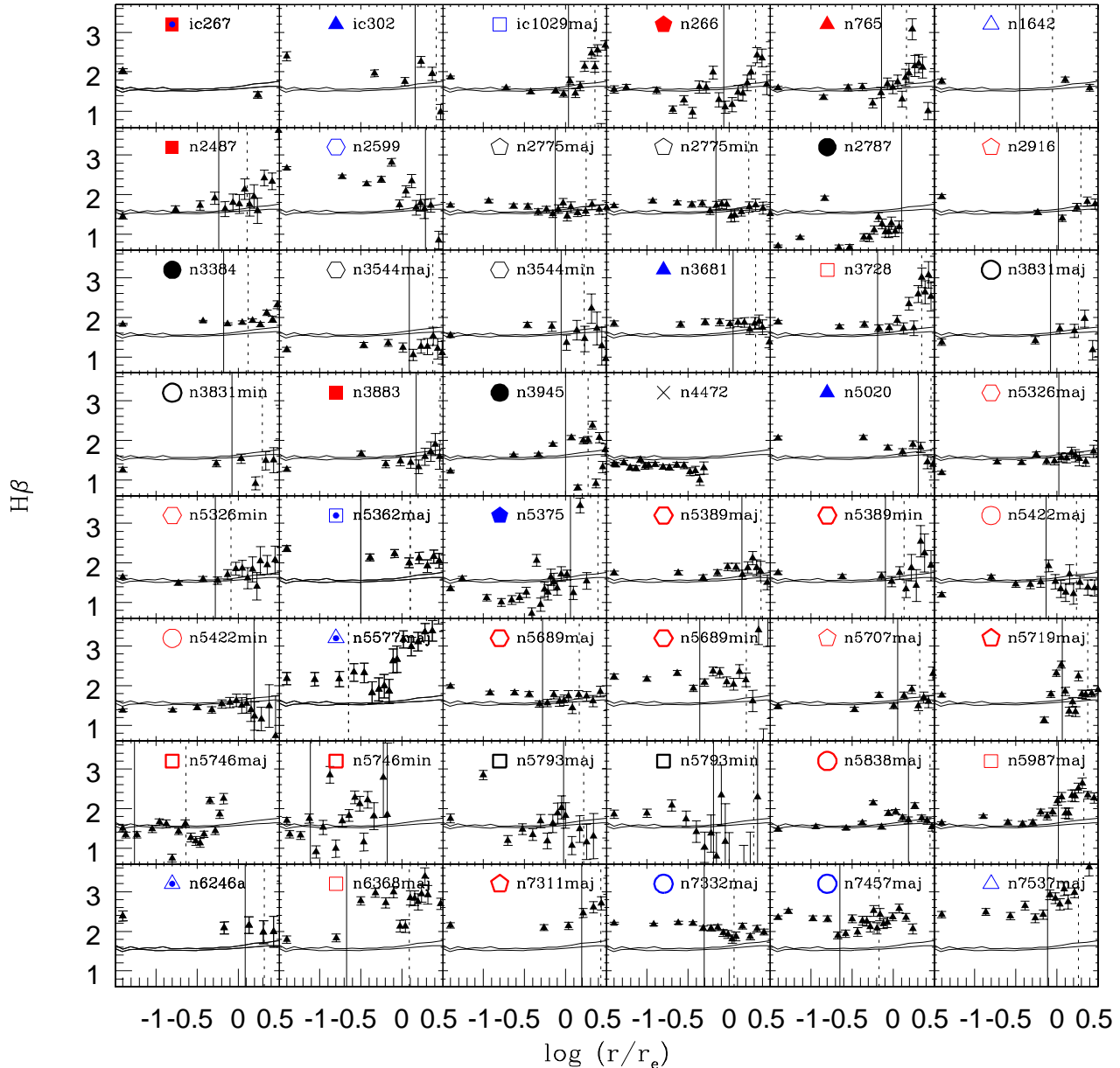


Figure 21. Comparison of $H\beta$ profiles between this work and merger models by Bekki & Shioya (1999) with initial disk masses of $10^{10}M_{\odot}$ (bottom curve) and $10^{12}M_{\odot}$. Symbols are as in Fig. 6.

els (Fig. 21). Nearly all our galaxies have flat $H\beta$ profiles within the bulge-dominated region as predicted by the models. The profiles of the oldest bulges agree with the models in their zero-points as well, while younger bulges lie above the models.

Through chemical evolution modeling, Thomas et al. (1999) studied α/Fe ratios in ellipticals that formed through a fast ($\bar{1}$ Gyr) collapse of star-forming clumps and through mergers of MW-like spirals. The main difference between the two models was that the merging spirals had several Gyr of Fe enrichment while the gas involved in the collapse was

not pre-enriched in Fe. The large central α/Fe ratios found in massive ellipticals were reproduced in the collapse model. The merger model does not produce super-solar α/Fe assuming a Salpeter IMF unless the merger happened early, before the progenitors acquired much Fe. Metallicity and α/Fe are anticorrelated in the collapse model; since ellipticals have negative gradients in metallicity, the model predicts that they should have a positive gradient in α/Fe . The merger model produces solar α/Fe in the outer regions. Therefore, uniformly solar α/Fe is consistent with the merger model while positive gradients are consistent with the collapse

model. Pipino et al. (2005) also find positive α/Fe gradients in a model where ellipticals are formed through the infall of gaseous lumps. Since our blue bulges have uniformly solar α/Fe , they are consistent with the predictions of the merger model. Several of the red bulges have positive gradients as predicted by the collapse model. Most of the remaining bulges have uniformly super-solar α/Fe , which is difficult to reproduce in any of the models.

In summary, both collapse and merger models have limited success in reproducing the line strength profiles of individual galaxies but neither explains the full range of behaviors seen in the data. It is important to note that hierarchical models are only beginning to make robust predictions for SPs, successfully reproducing properties traditionally thought to favor the collapse model, such as the mass-metallicity relation. As advancements continue to be made in incorporating gas dynamics, star formation, and chemical evolution in cosmologically-motivated merger models, it will be interesting to see if the line strength profiles will be reproduced as well.

5.1 Mergers

In a recent paper, Faber et al. (2005) argued that massive red ellipticals could not have formed entirely through major mergers of gas-rich components or through dry mergers but through a combination of the two. Ellipticals of the same mass and color could have formed in different ways: through early gas-rich mergers of low-mass objects followed by dry mergers or through recent gas-rich mergers of more massive objects. Objects that arrived on the red sequence early-on and have been gaining mass through dry mergers will have larger SSP ages than those that have arrived on the red sequence near their present mass as the result of recent gas-rich mergers. The former will also have smaller metallicities since their last gas-rich mergers were of lower mass progenitors with correspondingly lower metallicities according to the gas-phase mass-metallicity relation (Kobulnicky et al. 2003; Tremonti et al. 2004). The predicted anticorrelation between age and metallicity at fixed σ_0 is seen in ellipticals. If such an anticorrelation exists for bulges, it is not nearly as tight as that of ellipticals. This suggests that an additional formation mechanism might be required to explain the SPs of bulges.

Recent semi-analytic models incorporating the Millennium Simulation of cosmic structure growth find a correlation between stellar metallicity and stellar mass, with the most massive galaxies having roughly solar metallicity (De Lucia et al. 2005). This is qualitatively consistent with the observed $[\text{MgFe}]'-\sigma_0$ and $[\text{MgFe}]'-V_{max}$ relations. Massive ellipticals and bulges have super-solar central metallicity which is in apparent contradiction with de Lucia et al.'s results. However, they also have negative metallicity gradients. The arrows in Fig. 15, which extend to approximately the bulge effective radius, fall around solar metallicity in the massive red bulges. The metallicity at the effective radius is more representative, than the central value, of the mean metallicity. Therefore, the data are not inconsistent with the models.

de Lucia et al. also find in their simulations that less massive ellipticals had more extended star formation histories than their massive counterparts. This is consistent with

the observed $\alpha/\text{Fe}-\sigma_0$ and $\alpha/\text{Fe}-V_{max}$ correlations. These correlations can be produced in starbursts induced by gas-rich mergers. During the starburst, SN II enrich the ISM with α -elements. If star-formation is somehow quenched before SN Ia contribute much Fe, the α/Fe ratio increases. Dry mergers would add scatter to the $\alpha/\text{Fe}-\sigma_0$ and $\alpha/\text{Fe}-V_{max}$ relations since they increase σ_0 and V_{max} without altering the α/Fe ratio.

The differences in between blue and red bulges at fixed σ_0 can also be explained by mergers. At fixed σ_0 , blue bulges have smaller SSP ages than their red counterparts which suggests that they have undergone gas-rich mergers more recently. The progenitors of the blue bulges have then had more time to acquire Fe. Since the progenitors have small α/Fe ratios, so do the remnants. This is seen in the simulations by Thomas et al. (1999), who found that gas-rich mergers cannot produce large α/Fe ratios unless they happened early in the chemical evolution of the progenitors.

5.2 Secular Evolution

In dissipationless secular evolution, the bulge is formed through the vertical and radial redistribution of disk stars. In this process, existing gradients can either become amplified since the resulting [pseudo]bulge has a smaller scale length than the progenitor disk or erased as a consequence of disk heating. But if the disk has no gradient, neither should the bulge. This process cannot be ruled out on the basis of $[\text{MgFe}]'$ gradients since the majority of galaxies show negative gradients in the disk-dominated region. However, the majority of red bulges have solar α/Fe in the disk-dominated region despite having super-solar α/Fe in the bulge. Therefore they could not have been produced through purely dissipationless secular evolution. If secular evolution with gas infall has been responsible for the formation of these objects, the star-formation timescales must have been identical (at fixed σ_0) in this scenario as in merger-induced star-formation since red bulges and ellipticals follow the same $\alpha/\text{Fe}-\sigma_0$ relation. Furthermore, the star formation must have been completed several Gyr ago since red bulges have large SSP ages. This goes for the three barred S0s with disk-like structural and kinematical properties (NGCs 2787, 3384, and 3945) as well. These objects are identical to ellipticals of comparable σ_0 in their stellar populations and two of them have among the largest central SSP ages observed.

Note that the α/Fe ratios of the blue bulges are consistent with dissipationless secular evolution. Unfortunately, neither mergers nor secular evolution can be ruled out for blue bulges on the basis of their α/Fe ratios.

Secular evolution with gas infall is supported by the frequency of barred galaxies with age gradients. Of the ten galaxies whose central regions are younger than the outer regions, seven are barred and one have a b/p bulge. Bar-driven gas infall could lead to extended star-formation in the central region, producing the observed age gradient.

If bars are long-lived and the chemical imprints of secular evolution are different from those of mergers, we would expect the bulges of barred galaxies to have different abundance patterns than those of unbarred galaxies. We see hints of such differences in index- σ_0 and index- V_{max} relations. At fixed σ_0 and V_{max} , barred galaxies appear to have larger central metallicities.

The metallicities of bulges and their disks are correlated. This is naturally explained in processes that involve the bulge being formed from the disk. However, this correlation holds for all galaxies, not just those with bars, blue bulges, or bulges identified as having disk-like structure and kinematics. Therefore either all bulges formed secularly and some had their bars destroyed or the other bulge/disk formation mechanisms also produce this correlation.

5.2.1 Evolution of Galaxy Populations

Small- σ bulges fall into two categories: YMR bulges with little or no star formation and MP bulges which are actively forming stars. This suggests that the MP bulges would have migrated to the YMR region by the time their star-formation is quenched. Will this be the scenario for all metal-poor bulges (including that of the Milky Way) or is the observed anticorrelation between emission strength and metallicity the result of small number statistics? Are there really no metal-poor bulges that do not have emission? Extending this type of study to large galaxy samples should shed light into the evolution of small- σ bulges.

While all five of the MP galaxies are late-types (Sb-Sc), three of the seven YMR galaxies are early types (S0-Sa). Perhaps, the mechanisms that trigger and quench the star-formation are also responsible for transforming galaxies from late- to early-types. As the YMR bulges age, they will move down to the OMR region.

6 SUMMARY

We have studied line strengths in the bulges and inner disks of 38 galaxies in the local universe. Our galaxies span a wide range of Hubble types, central velocity dispersions, maximum disk rotational velocities, and inclinations. The low-inclination galaxies include barred and unbarred objects; the edge-on galaxies include those with and without boxy/peanut-shaped bulges. We included several galaxies whose bulges were previously identified as being disk-like in their colors or kinematics to see if their spectral properties reveal evidence for secular evolution. We use the [MgFe]' index and five Balmer indices to characterize the luminosity-weighted metallicities and ages of the SPs and the Mgb/⟨Fe⟩ index to characterize the α /Fe ratios. Our main results are the following:

- The central regions of bulges range in SSP metallicity from $[Z/H]=-0.8$ to $+0.7$ dex and in SSP age from less than 2 to greater than 15 Gyr.
- The central ages and metallicities are sensitive to bulge color which is in turn sensitive to central velocity dispersion and maximum disk rotational velocity.
- Red bulges of all Hubble types are similar to luminous ellipticals in their central SPs. They have large SSP ages and are super-solar in SSP metallicity and α /Fe.
- Blue bulges can be separated into two classes: a metal-poor class that is restricted to late-types with small velocity dispersion and a young, metal-rich class that includes all Hubble types and velocity dispersions. The metal-poor blue bulges are actively forming stars while the metal-rich ones are not. Low-luminosity ellipticals exhibit a similar range of SSP ages and metallicities as blue bulges.

- Luminous ellipticals and the different types of bulges form a continuous and overlapping sequence on diagrams of metallicity- and age-sensitive indices versus σ_0 . At fixed σ_0 , there is no systematic difference between bulges and ellipticals on these diagrams but bulges exhibit larger scatter. At fixed σ_0 , age and metallicity are more tightly anticorrelated in ellipticals than in bulges.

- α /Fe in red bulges is correlated with σ_0 and V_{max} . Red bulges and ellipticals follow the same α /Fe- σ_0 relation.

- Most blue bulges (11 out of 14) are consistent with having solar α /Fe. At fixed σ_0 , blue bulges have smaller α /Fe than red bulges and ellipticals.

- Barred galaxies appear to have larger central metallicities than unbarred galaxies of the same σ_0 and V_{max} .

- Most galaxies show a steady decrease in metallicity-sensitive indices with radius. The slope of the gradient is correlated with the central value and therefore with the global kinematics. The bulge- and disk-dominated regions are distinct in their line strength profiles, with the disks generally having shallower slopes. The smallest bulges do not have negative line strength gradients; some of these have flat profiles in the central region while others have positive gradients.

- There is a correlation between [MgFe]' strength in the bulge and the disk. This correlation holds for all galaxies, not just those with bars, blue bulges, or bulges identified as having disk-like structural or kinematical properties.

- Where positive age gradients (with the central regions being younger) are present, they are invariably in barred galaxies. This suggests that bar-driven star formation has occurred. However, several red bulges in barred galaxies have large central SSP ages (although it could be younger than the outer regions) which means there has been no significant bar-driven star formation for several Gyr.

- Four galaxies have super-solar α /Fe in the disk-dominated region. The rest are consistent with having solar α /Fe in the disk.

- Objects identified as having disk-like structural or kinematic properties do not have noticeably different SPs than other bulges. They follow the same scaling relations as the red bulges and ellipticals and have metallicity gradients. The three barred S0s identified as having bulges with disk-like structural and kinematic properties are also α -enhanced and therefore do not resemble the majority of the disks, including the MW disk at the solar neighborhood.

- Color profiles agree frequently but not always with line strength profiles. Where there is a discrepancy, due likely to the colors being affected by dust, it is usually in the central regions. Consequently, color gradients (computed as the difference in color between the center and a characteristic scale length) do not necessarily correlate with [MgFe]' gradients, illustrating the value of spectroscopy.

Overall, our results are consistent with the hypothesis that mergers have been the dominant mechanism responsible for the formation of bulges. However, some of the observations, such as the correlation between bulge and disk metallicity, pose significant challenges to the merger scenario. Furthermore, the possibility that barred galaxies follow different scaling relations than unbarred galaxies and are overrepresented among galaxies with age gradients supports the secular evolution picture.

Central line strengths on a statistically significant sample of ellipticals and bulges of barred and unbarred spirals would be invaluable in determining whether more than one formation mechanism is required for bulges. The necessary data are already available in the databases of large surveys such as the SDSS. Spatially resolved studies on a smaller, representative sample, would allow for better comparisons between gradients in different types of galaxies.

7 ACKNOWLEDGEMENTS

It is a pleasure to thank Anatoly Klypin, Jason Peterson, Jesus Falc3n-Barroso, Reynier Peletier, Claudia Maraston, Daniel Thomas, Scott Trager, and Guy Worthey for helpful discussions or assistance with the data analysis. Partial funding was provided by the New Mexico Space Grant Consortium. This research has made use of the NASA/IPAC Extragalactic Database (NED) which is operated by the Jet Propulsion Laboratory, California Institute of Technology, under contract with the National Aeronautics and Space Administration.

REFERENCES

- Abadi M. G., Navarro J. F., Steinmetz M., Eke V. R., 2003, *ApJ*, 597, 21
- Angeletti L., Giannone P., 2003, *A&A*, 403, 449
- Arimoto N., Yoshii Y., 1987, *A&A*, 173, 23
- Aronica G., Athanassoula E., Bureau M., Bosma A., Dettmar R.-J., Vergani D., Pohlen M., 2003, *AP&SS*, 284, 753
- Athanassoula E., 2005, *MNRAS*, 358, 1477
- Athanassoula E., Misiriotis A., 2002, *MNRAS*, 330, 35
- Balcells M., Graham A. W., Domínguez-Palmero L., Peletier R. F., 2003, *ApJ*, 582, L79
- Balcells M., Peletier R. F., 1994, *AJ*, 107, 135
- Baldwin J. A., Phillips M. M., Terlevich R., 1981, *PASP*, 93, 5
- Bekki K., Shioya Y., 1999, *ApJ*, 513, 108
- Bell E. F., Wolf C., Meisenheimer K., Rix H.-W., Borch A., Dye S., Kleinheinrich M., Wisotzki L., McIntosh D. H., 2004, *ApJ*, 608, 752
- Bender R., Burstein D., Faber S. M., 1993, *ApJ*, 411, 153
- Bertola F., Capaccioli M., 1977, *ApJ*, 211, 697
- Bournaud F., Combes F., Semelin B., 2005, *MNRAS*, pp L89+
- Bruzual G., Charlot S., 2003, *MNRAS*, 344, 1000
- Bureau M., Freeman K. C., 1999, *AJ*, 118, 126
- Burstein D., Faber S. M., Gaskell C. M., Krumm N., 1984, *ApJ*, 287, 586
- Busarello G., Capaccioli M., D’Onofrio M., Longo G., Richter G., Zaggia S., 1996, *A&A*, 314, 32
- Caldwell N., Rose J. A., Concannon K. D., 2003, *AJ*, 125, 2891
- Cappellari M., Emsellem E., 2004, *PASP*, 116, 138
- Carlberg R. G., 1984, *ApJ*, 286, 403
- Carollo C. M., Danziger I. J., Buson L., 1993, *MNRAS*, 265, 553
- Carollo C. M., Stiavelli M., de Zeeuw P. T., Mack J., 1997, *AJ*, 114, 2366
- Chung A., Bureau M., 2004, *AJ*, 127, 3192
- Combes F., Debbasch F., Friedli D., Pfenniger D., 1990, *A&A*, 233, 82
- Courteau S., de Jong R. S., Broeils A. H., 1996, *ApJ*, 457, L73
- Davidge T. J., 2001, *AJ*, 122, 1386
- de Jong R. S., 1996, *A&A*, 313, 377
- de Jong R. S., Simard L., Davies R. L., Saglia R. P., Burstein D., Colless M., McMahan R., Wegner G., 2004, *MNRAS*, 355, 1155
- De Lucia G., Springel V., White S. D. M., Croton D., Kauffmann G., 2005, *ArXiv e-prints (astro-ph/0509725)*
- de Vaucouleurs G., de Vaucouleurs A., Corwin H. G., Buta R. J., Paturel G., Fouque P., 1991, *Third Reference Catalogue of Bright Galaxies*. Volume 1-3, XII, 2069 pp. 7 figs.. Springer-Verlag Berlin Heidelberg New York
- Debbasch F., Carollo C. M., Mayer L., Moore B., 2004, *ApJ*, 604, L93
- Denicol3 G., Terlevich R., Terlevich E., Forbes D. A., Terlevich A., 2005, *MNRAS*, 358, 813
- Denicol3 G., Terlevich R., Terlevich E., Forbes D. A., Terlevich A., Carrasco L., 2005, *MNRAS*, 356, 1440
- Eisenstein D. J., Hogg D. W., Fukugita M., Nakamura O., Bernardi M., Finkbeiner D. P., Schlegel D. J., Brinkmann J., Connolly A. J., Csabai I., Gunn J. E., Ivezić Ž., Lamb D. Q., Loveday J., Munn J. A., Nichol R. C., Schneider D. P., Strauss M. A., Szalay A., York D. G., 2003, *ApJ*, 585, 694
- Emsellem E., Cappellari M., Peletier R. F., McDermid R. M., Bacon R., Bureau M., Copin Y., Davies R. L., Krajnović D., Kuntschner H., Miller B. W., Tim de Zeeuw P., 2004, *MNRAS*, 352, 721
- Erwin P., Beltrán J. C. V., Graham A. W., Beckman J. E., 2003, *ApJ*, 597, 929
- Faber S. M., Friel E. D., Burstein D., Gaskell C. M., 1985, *ApJS*, 57, 711
- Faber S. M., Willmer C. N. A., Wolf C., Koo D. C., Weiner B. J., Newman J. A., Im M., Coil A. L., Conroy C., Cooper M. C., Davis M., Finkbeiner D. P., Gerke B. F., Gebhardt K., Groth E. J., Guhathakurta P., Harker J., Kaiser N., Kassin S., Kleinheinrich M., Konidaris N. P., Lin L., Lupino G., Madgwick D. S., Noeske K. M. K. G., Phillips A. C., Sarajedini V. L., Simard L., Szalay A. S., Vogt N. P., Yan R., 2005, *ArXiv e-prints astro-ph/0506044*
- Fairall A. P., Willmer C. N. A., Calderon J. H., Latham D. W., Nicolaci da Costa L., Pellegrini P. S., Nunes M. A., Focardi P., Vettolani G., 1992, *AJ*, 103, 11
- Falc3n-Barroso J., Peletier R. F., Balcells M., 2002, *MNRAS*, 335, 741
- Falc3n-Barroso J., Peletier R. F., Emsellem E., Kuntschner H., Fathi K., Bureau M., Bacon R., Cappellari M., Copin Y., Davies R. L., de Zeeuw T., 2004, *MNRAS*, 350, 35
- Feltzing S., Gilmore G., 2000, *A&A*, 355, 949
- Ferreiro D. L., Pastoriza M. G., 2004, *A&A*, 428, 837
- Fisher D., Franx M., Illingworth G., 1996, *ApJ*, 459, 110+
- Forbes D. A., Sánchez-Blázquez P., Proctor R., 2005, *MNRAS*, pp L47+
- Friedli D., Benz W., 1995, *A&A*, 301, 649
- Gadotti D. A., dos Anjos S., 2001, *AJ*, 122, 1298
- Goudfrooij P., Gorgas J., Jablonka P., 1999, *AP&SS*, 269, 109
- Ibata R. A., Gilmore G. F., 1995, *MNRAS*, 275, 605

- Idiart T. P., de Freitas Pacheco J. A., Costa R. D. D., 1996, *AJ*, 112, 2541
- Immeli A., Samland M., Gerhard O., Westera P., 2004, *A&A*, 413, 547
- Jablonka P., Courbin F., Meylan G., Sarajedini A., Bridges T. J., Magain P., 2000, *A&A*, 359, 131
- Jablonka P., Gorgas J., Goudfrooij P., 2002, *AP&SS*, 281, 367
- Jablonka P., Martin P., Arimoto N., 1996, *AJ*, 112, 1415
- Kannappan S. J., Jansen R. A., Barton E. J., 2004, *AJ*, 127, 1371
- Karachentsev I. D., Makarov D. A., 1996, *AJ*, 111, 794
- Kauffmann G., Heckman T. M., Tremonti C., Brinchmann J., Charlot S., White S. D. M., Ridgway S. E., Brinkmann J., Fukugita M., Hall P. B., Ivezić Ž., Richards G. T., Schneider D. P., 2003, *MNRAS*, 346, 1055
- Kauffmann G., White S. D. M., Guiderdoni B., 1993, *MNRAS*, 264, 201+
- Kobayashi C., Arimoto N., 1999, *ApJ*, 527, 573
- Kobulnicky H. A., Willmer C. N. A., Phillips A. C., Koo D. C., Faber S. M., Weiner B. J., Sarajedini V. L., Simard L., Vogt N. P., 2003, *ApJ*, 599, 1006
- Kormendy J., 1993, in *IAU Symp. 153: Galactic Bulges Kinematics of extragalactic bulges: evidence that some bulges are really disks.* pp 209–+
- Kormendy J., Illingworth G., 1982, *ApJ*, 256, 460
- Kormendy J., Kennicutt R. C., 2004, *ARA&A*, 42, 603
- Lütticke R., Dettmar R.-J., Pohlen M., 2000, *A&AS*, 145, 405
- Larson R. B., 1974, *MNRAS*, 166, 585
- Lee H.-c., Worthey G., 2005, *ApJS*, 160, 176
- MacArthur L. A., 2005, *ApJ*, 623, 795
- MacArthur L. A., Courteau S., Holtzman J. A., 2003, *ApJ*, 582, 689
- Massey P., Strobel K., Barnes J. V., Anderson E., 1988, *ApJ*, 328, 315
- Michard R., Marchal J., 1994, *A&AS*, 107, 187
- Minniti D., 1996, *ApJ*, 459, 175
- Nilson P., 1973, *Uppsala general catalogue of galaxies. Acta Universitatis Upsaliensis. Nova Acta Regiae Societatis Scientiarum Upsaliensis - Uppsala Astronomiska Observatoriums Annaler, Uppsala: Astronomiska Observatorium, 1973*
- Noguchi M., 2000, *MNRAS*, 312, 194
- Norman C. A., Sellwood J. A., Hasan H., 1996, *ApJ*, 462, 114
- Peletier R. F., Balcells M., 1997, *New Astronomy*, 1, 349
- Peletier R. F., Vazdekis A., Arribas S., del Burgo C., García-Lorenzo B., Gutiérrez C., Mediavilla E., Prada F., 1999, *MNRAS*, 310, 863
- Pfenniger D., 1993, in *Galactic Bulges, IAU Symposium 153, (H. Dejonghe & H.J. Habing eds.), Kluwer, Dordrecht, p. 387-390 Delayed Formation of Bulges by Dynamical Processes.* pp 387–390
- Pinkney J., Gebhardt K., Bender R., Bower G., Dressler A., Faber S. M., Filippenko A. V., Green R., Ho L. C., Kormendy J., Lauer T. R., Magorrian J., Richstone D., Tremaine S., 2003, *ApJ*, 596, 903
- Proctor R. N., Sansom A. E., 2002, *MNRAS*, 333, 517
- Proctor R. N., Sansom A. E., Reid I. N., 2000, *MNRAS*, 311, 37
- Prugniel P., Maubon G., Simien F., 2001, *A&A*, 366, 68
- Puzia T. H., Perrett K. M., Bridges T. J., 2005, *A&A*, 434, 909
- Puzia T. H., Saglia R. P., Kissler-Patig M., Maraston C., Greggio L., Renzini A., Ortolani S., 2002, *A&A*, 395, 45
- Raimann D., Storchi-Bergmann T., Bica E., Alloin D., 2001, *MNRAS*, 324, 1087
- Raimann D., Storchi-Bergmann T., González Delgado R. M., Cid Fernandes R., Heckman T., Leitherer C., Schmitt H., 2003, *MNRAS*, 339, 772
- Rich R. M., 1999, in *ASP Conf. Ser. 192: Spectrophotometric Dating of Stars and Galaxies Age and Metallicity of the Bulges of the Milky Way and M31.* pp 215–+
- Rose J. A., Bower R. G., Caldwell N., Ellis R. S., Sharples R. M., Teague P., 1994, *AJ*, 108, 2054
- Ryder S. D., Fenner Y., Gibson B. K., 2005, *MNRAS*, 358, 1337
- Sadler E. M., Rich R. M., Terndrup D. M., 1996, *AJ*, 112, 171
- Sarajedini A., Jablonka P., 2005, *AJ*, 130, 1627
- Sellwood J. A., 1993, in *IAU Symp. 153: Galactic Bulges Peanut shaped bars.* pp 391–+
- Shen J., Sellwood J. A., 2004, *ApJ*, 604, 614
- Sil'chenko O. K., Afanasiev V. L., Chavushyan V. H., Valdes J. R., 2002, *ApJ*, 577, 668
- Sil'chenko O. K., Moiseev A. V., Afanasiev V. L., Chavushyan V. H., Valdes J. R., 2003, *ApJ*, 591, 185
- Stephens A. W., Frogel J. A., DePoy D. L., Freedman W., Gallart C., Jablonka P., Renzini A., Rich R. M., Davies R., 2003, *AJ*, 125, 2473
- Tanvir N. R., Ferguson H. C., Shanks T., 1999, *MNRAS*, 310, 175
- Thomas D., Maraston C., Bender R., 2003, *MNRAS*, 339, 897
- Thomas D., Maraston C., Bender R., de Oliveira C. M., 2005, *ApJ*, 621, 673
- Thomas D., Maraston C., Korn A., 2004, *MNRAS*, 351, L19
- Trager S. C., Faber S. M., Worthey G., González J. J., 2000a, *AJ*, 119, 1645
- Trager S. C., Faber S. M., Worthey G., González J. J., 2000b, *AJ*, 120, 165
- Trager S. C., Worthey G., Faber S. M., Burstein D., Gonzalez J. J., 1998, *ApJS*, 116, 1
- Tremonti C. A., Heckman T. M., Kauffmann G., Brinchmann J., Charlot S., White S. D. M., Seibert M., Peng E. W., Schlegel D. J., Uomoto A., Fukugita M., Brinkmann J., 2004, *ApJ*, 613, 898
- Tripicco M. J., Bell R. A., 1995, *AJ*, 110, 3035
- van Dokkum P. G., 2005, *ArXiv e-prints (astro-ph/0506661)*
- van Dokkum P. G., Franx M., Fabricant D., Kelson D. D., Illingworth G. D., 1999, *ApJ*, 520, L95
- van Loon J. T., Gilmore G. F., Omont A., Blommaert J. A. D. L., Glass I. S., Messineo M., Schuller F., Schultheis M., Yamamura I., Zhao H. S., 2003, *MNRAS*, 338, 857
- Vazdekis A., 1999, *ApJ*, 513, 224
- Vazdekis A., Kuntschner H., Davies R. L., Arimoto N., Nakamura O., Peletier R., 2001, *ApJ*, 551, L127
- Vazdekis A., Peletier R. F., Beckman J. E., Casuso E., 1997, *ApJS*, 111, 203
- Wegner G., da Costa L. N., Alonso M. V., Bernardi M.,

- Wilmer C. N. A., Pellegrini P. S., Rit e C., Maia M., 2000, in ASP Conf. Ser. 201: Cosmic Flows Workshop The Nearby Early-type Galaxies Survey (ENEAR): Project Description and Some Preliminary Results. pp 62–+
- Worthey G., 1994, ApJS, 95, 107
- Worthey G., Collobert M., 2003, ApJ, 586, 17
- Worthey G., Faber S. M., Gonzalez J. J., Burstein D., 1994, ApJS, 94, 687
- Worthey G., Ottaviani D. L., 1997, ApJS, 111, 377
- Wyse R. F. G., Gilmore G., Franx M., 1997, ARA&A, 35, 637
- Zoccali M., Renzini A., Ortolani S., Greggio L., Saviane I., Cassisi S., Rejkuba M., Barbuy B., Rich R. M., Bica E., 2003, A&A, 399, 931

Table 1. The Galaxy Sample. DJ denotes de Jong (1996), PB denotes Peletier & Balcells (1996), and EN denotes the ENEAR survey (Wegner et al. 2000). Morphological types are from the NASA/IPAC Extragalactic Database. B magnitudes are from RC3 (de Vaucouleurs et al. 1991). Bulge and disk colors are from DJ and PB. Bulge color is defined to be the color at half the K-band bulge effective radius or 5 arcsec, whichever is larger. Disk color is defined to be the color at two disk scale lengths. b/a is the red major over minor axis ratio taken from the sources listed. The recessional velocities shown are the RC3 heliocentric velocities corrected to the Local Group according to Karachentsev & Makarov (1996). Where both 21cm and optical velocities were available, the 21 cm values were used. Since no RC3 data was available for NGC 3831, the B magnitude and optical heliocentric velocity were taken from Fairall et al. (1992). The scale was obtained assuming $H_0=70$. The distance to NGC 3384 was determined by Cepheid observations (Tanvir et al. 1999).

Galaxy	Source	Type	Morph.	m_B (mag)	$(B-K)_B$	$(B-R)_D$	b/a	V_{LG} (km/s)	Scale (kpc/arcsec)
IC 267	DJ	SBb	Bar	13.63	4.6	4.24	0.71	3577	0.25
IC 302	DJ	SBbc	Bar	13.59			0.92	5950	0.41
IC 1029	PB	SAb	Ell*	13.64	3.89	3.77	0.24	2520	0.17
NGC 266	DJ	SBab	Bar	12.33	4.6	3.85	0.94	4908	0.34
NGC 765	DJ	SABbc	Bar	13.60	4.4	3.82	1.00	5117	0.37
NGC 1642	DJ	SA(rs)c	Unb?	13.28	4.0	3.26	1.00	4579	0.32
NGC 2487	DJ	SBb	Bar	13.10	4.1	3.53	0.92	4758	0.33
NGC 2599	DJ	SAA	Unb	13.12	4.0	3.8	1.00	4651	0.32
NGC 2775	EN	SAab	Unb	11.13			0.85	1173	0.08
NGC 2787		SB0+	Bar	11.77				696	0.06
NGC 2916	DJ	SAab	Unb	12.42	4.2	3.59	0.74	3618	0.25
NGC 3384		SB0-	Bar	10.63				735	0.06
NGC 3544	EN	SABA	Unb?	12.99			0.30	3354	0.23
NGC 3681	DJ	SAB(r)bc	Bar	12.25	3.8	3.47	1.00	1239	0.08
NGC 3728	DJ	SAb	Unb	13.80	4.2	3.7	0.75	6904	0.48
NGC 3831	EN	SAB0+	Box*	14.5			0.24	4715	0.33
NGC 3883	DJ	SAb	Bar	13.10	4.1	3.44	0.91	6937	0.48
NGC 3945		SB0+	Bar	11.38				1220	0.09
NGC 4472	EN	E2		9.30				744	0.05
NGC 5020	DJ	SABbc	Bar	12.50	3.6	3.11	0.85	3284	0.23
NGC 5326	PB	SAA	Unb	12.92	4.05	3.97	0.50	2573	0.18
NGC 5362	PB	SAb	Unb	13.14	3.56	3.24	0.37	2314	0.16
NGC 5375	DJ	SBab	Bar	12.40	3.9	3.47	0.81	2418	0.17
NGC 5389	PB	SAB0/a	Box*	13.10	4.12	4.10	0.20	1996	0.14
NGC 5422	PB	SA0	Ell*	12.81	4.17	4.09	0.20	1921	0.13
NGC 5577	PB	SAbc	Ell*	13.05	3.84	3.54	0.28	1702	0.12
NGC 5689	PB	SBO/a	Box?*	12.54	4.14	4.12	0.25	2295	0.16
NGC 5707	PB	SAab	Ell*	13.38	4.24	3.92	0.25	2354	0.16
NGC 5719	PB	SABab	Box?*	13.1	4.54	3.84	0.36	1676	0.12
NGC 5746	PB	SABb	Pea*	11.38	4.42	4.50	0.16	1676	0.12
NGC 5793	EN	SABb	Box?	14.30			0.37	3387	0.23
NGC 5838	PB	SA0-	Box?*	11.74	4.21	4.11	0.35	1338	0.09
NGC 5987	PB	SAb	Ell	13.00	4.46	4.14	0.40	3207	0.22
NGC 6246A	DJ	SABc	Unb	14.10	3.9	3.23	0.91	5495	0.38
NGC 6368	PB	SAb	Ell*	13.10	4.84	4.58	0.20	2904	0.20
NGC 7311	PB	SAab	Ell	13.36	4.35	4.07	0.50	4762	0.33
NGC 7332	PB	SAB0	Box*	12.11	3.75	3.58	0.26	1584	0.11
NGC 7457	PB	SAB0-	Box?	11.86	3.69	3.50	0.52	1115	0.08
NGC 7537	PB	SAbc	Ell*	13.65	3.88	3.62	0.34	2888	0.20

Table 2. Spectrograph specifications during our observing runs

Detector	Obs. Dates (M/D/Y)	Grating	Disp. ($\text{\AA}/\text{pix}$)	Approx. Resol. (\AA)	Scale (Arcsec/pix)
DIS I Blue	1/10/00-2/11/02	Med	3.18	5.7	1.086
DIS I Red	1/10/00-2/11/02	Med	3.53	8.6	0.605
DIS II Blue	4/13/02-10/09/02	Low	3.05	8.6	0.600
DIS II Red	4/13/02-04/07/03	Med	3.13	7.8	0.605
DIS III Blue	03/06/03-02/15/04	Low	2.42	7.7	0.419
DIS III Red	05/29/03-02/15/04	Med	2.31	6.9	0.396

Table 3. Spectroscopic Observations

Galaxy	Axis	PA	Date (M/D/Y)	Exp. Time (Sec)
IC 267	Bar	-25	12/22/03	1x2400
				1x1230
IC 302	Bar	8	10/9/02	2x2400
IC 1029	Maj	152	5/30/03	3x2400
NGC 266	Bar	0	9/17/02	2x2400
NGC 765		15	12/22/03	3x2400
NGC 1642	Bar	0	12/1/03	2x2400
NGC 2487		45	2/11/02	3x2400
NGC 2599	Maj	-90	2/11/02	3x2400
NGC 2775		66	1/10/00	3x1200
NGC 2787	Min	156	1/10/00	3x1200
	Maj	109	2/15/04	2x2400
NGC 2916	Min	-80	12/1/03	2x2400
				1x900
NGC 3384	Maj	50	2/15/04	2x2400
NGC 3544	Maj	-84	1/10/00	3x1200
	Min	6	4/25/00	3x1200
NGC 3681	Bar	-25	2/11/02	3x2400
NGC 3728	Maj	20	3/6/03	3x2400
NGC 3831	Maj	24	4/25/00	3x1200
	Min	114	5/3/00	3x1800
NGC 3883	Maj	-14	3/7/03	3x2400
				1x1200
NGC 3945	Maj	-22	2/15/04	2x2400
				1x1800
NGC 4472		67	1/10/00	3x1200
NGC 5020	Bar	38	3/6/03	2x2400
NGC 5326	Maj	-44	5/4/00	4x1800
	Min	-134	2/11/02	2x2400
NGC 5362	Maj	-92	6/16/01	4x2400
NGC 5375	Bar	-10	4/7/03	1x2400
				1x1200
NGC 5389	Maj	3	5/2/00	4x1800
	Min	-87	5/2/00	3x1800
NGC 5422	Maj	-26	5/2/00	2x1200
	Min	64	5/3/00	2x1800
NGC 5577	Maj	56	1/10/00	2x1500
				3x1200
NGC 5689	Maj	-93	6/17/01	3x2400
	Min	0	4/13/02	2x2400
NGC 5707	Maj	39	5/29/03	2x2400
				1x1200
NGC 5719	Maj	-90	5/30/03	3x2400
NGC 5746	Maj	-9	4/17/02	3x2400
	Min	-99	4/17/02	3x2400
NGC 5793	Maj	-35	5/4/00	1x1800
	Min	55		2x1500
NGC 5838	Maj	42	6/8/02	2x2400
NGC 5987	Maj	-109	5/30/03	1x2400
				1x2700
NGC 6246A		-90	2/19/01	2x1800
			2/20/01	2x1800
NGC 6368	Maj	47	6/29/03	1x2400
				1x2100
NGC 7311	Maj	24	7/1/03	1x2400
		15	10/12/01	1x2400
NGC 7332	Maj	-24	7/3/00	4x1800
NGC 7457	Maj	-38	1x2400	1x1257
				4x2400
NGC 7537	Maj	-100	10/12/01	4x2400